High contribution of new particle formation to ultrafine particles in four seasons in an urban atmosphere in south China

Li Tao[1], Zhen Zhou[2], Jun Tao[1,8*], Leiming Zhang[3], Cheng Wu[4], Jiawei Li[5], Dingli Yue[6], Zhijun Wu[7], Zhisheng Zhang[8], Ziyang Yuan[9], Junjun Huang[1], Boguang Wang[1]

[1]Institute for Environmental and Climate Research, Jinan University, Guangzhou, China

[2]Dongguan Sub-branch of Guangdong Ecological and Environmental Monitoring Center, Dongguan, China

[3]Air Quality Research Division, Science and Technology Branch, Environment and Climate Change Canada, Toronto, Canada

[4]Institute of Mass Spectrometer and Atmospheric Environment, Jinan University, Guangzhou, China

[5]RCE-TEA, Institute of Atmospheric Physics, Chinese Academy of Sciences, Beijing, China

[6]Guangdong Ecological and Environmental Monitoring Center, Guangzhou, China

[7]State Key Joint Laboratory of Environmental Simulation and Pollution Control, College of Environmental Sciences and Engineering, Peking University, Beijing, China

[8]South China Institute of Environmental Sciences, Ministry of Ecology and Environment, Guangzhou, China

[9]Sailbri Cooper Inc., Tigard, Oregon, United States

*Correspondence author: (Jun Tao) taojun@jnu.edu.cn

Abstract. Ultra fine particles (UFP) cover the size range of both nucleation mode particles (NUC, D_p<25 nm) and Aitken mode particles (AIT, 25 nm < D_p <100 nm), and play important roles in radiative forcing and human health. In this study, we identified new particle formation (NPF) events and undefined events, explored their potential formation mechanism, and quantified their contributions to UFP number concentration (N_{UFP}) in urban Dongguan of the Pearl River Delta (PRD) region. Field campaigns were carried out in four seasons in 2019 to measure particle number concentration in the size range of 4.7-673.2nm, volatile organic compounds (VOCs), gaseous pollutants, chemical compositions in $PM_{2.5}$, and meteorological parameters. The frequency of the occurrence of NPF, as indicated by a significant increase in NUC number concentration (N_{NUC}), was 26%, and that of the undefined event, as indicated by substantial increases in N_{NUC} or AIT number concentration (N_{AIT}), was 32% during the whole campaign period. The NPF events mainly occurred in autumn (with a frequency of 59%) and winter (33%) and only occasionally in spring (4%) and summer (4%). On the contrary, the frequencies of the undefined events were higher in spring (52%) and summer (38%) than in autumn (19%) and winter (22%). The burst periods of the NPF events mainly occurred before 11:00 Local Time (LT), while those of the undefined events mainly occurred after 11:00 LT. Accompanied to NPF events were low concentrations of VOCs and high concentrations of O_3. The undefined events by NUC or AIT were associated with the upwind transport of newly formed particles. Source apportionment analysis suggested that NPF and undefined events were the largest contributor to N_{NUC} (51±28%), N_{AIT} (41±26%), and N_{UFP} (45±27%), while coal combustion and biomass burning, and traffic emission were the second largest contributor to N_{NUC} (22±20%) and N_{AIT} (39±28%), respectively.

Keywords: nucleation mode particle; Aitken mode particle; upwind transport; traffic emission; coal combustion; biomass burning

1. Introduction

Ultrafine particles (UFP, with an electrical mobility diameter (D_p) smaller than 100 nm) accounted for 80%-90% of total particle number concentration in urban environments (Mejía et al., 2008; Salma et al., 2011). UFP is an essential source of droplet mode particles and cloud condensation nuclei, and plays key role in haze formation, cloud formation, and radiative forcing (Guo et al., 2014; Junkermann and Hacker, 2018; Kulmala et al., 2021, 2022; Mishra et al., 2023; Peng et al., 2021). UPF also has a marked impact on human health via deep penetration into the lungs and blood systems (Schraufnagel, 2020). Traffic emission is an important source of UFP, which could contribute about 44%-71% of UFP number concentration (N_{UFP}) in urban and roadside environments (Brines et al., 2015; Rivas et al., 2020; Sowlat et al., 2016). Another important source of UFP is through new particle formation (NPF) processes.

UFP covers the particle size range of both nucleation mode particles (NUC, D_p<25 nm) and Aitken mode particles (AIT, 25 nm < D_p <100 nm). Available literature reported NUC number concentration (N_{NUC}) and AIT number concentration (N_{AIT}) account for about 18-32% and 68-82%, respectively, of N_{UFP} (Kanawade et al., 2014; Németh et al., 2018; Zhang et al., 2017). However, a number fraction as high as 40% of N_{NUC} in N_{UFP} was also reported on days with NPF events (Yadav et al., 2021). On days with undefined events, which were caused mainly by regional transport or the aging process of newly formed particles (Buenrostro Mazon et al., 2009), N_{NUC} and N_{AIT} equally contributed to N_{UFP} (Varanda Rizzo et al., 2018).

High frequencies of NPF events have been reported in China, e.g., in the PRD region (23%), the Yangtze River Delta region (YRD) (27%), and the North China Plain (NCP) (34%) (Zhang et al., 2021), which have drawn increasing attention of UFP on the environmental, climate and health impacts (Kulmala et al., 2021; Kulmala et al.,

2022; Lin et al., 2021; Tang et al., 2021). The NPF events, besides traffic emission (Liu et al., 2014; Wang et al., 2013b; Wu et al., 2021; Zhang et al., 2022), are responsible for the higher number fractions of N_{NUC} and N_{AIT} in N_{UFP} in these regions (Huang et al., 2022; Shang et al., 2023; Zhao et al., 2021). To date, few studies have systematically explored the formation mechanisms of the NPF and undefined events or quantified their contributions to N_{UFP} in the PRD region (Gong et al., 2010; Liang et al., 2021; Liu et al., 2008; Tan et al., 2016; Yue et al., 2013).

To fill these knowledge gaps, an integrated campaign was conducted in four seasons in 2019 in urban Dongguan, one of the cities in the PRD region with the highest number concentrations of fine particles (Huang et al., 2017; Tan et al., 2016). The particle number size distributions (4.7-637 nm), volatile organic compounds (VOCs), gaseous pollutants (SO_2, HONO, O_3, NO_2), dominant chemical compositions (OC, EC and elements) in $PM_{2.5}$, and meteorological parameters were measured synchronously. The occurrence frequencies and formation mechanisms of the NPF and undefined events and the sources of N_{UFP}, $N_{NUC,}$ and N_{AIT} were analyzed. Knowledge generated from this study will be helpful for formulating effective reduction strategies for fine particles in this region.

2. Methodology

2.1. Sampling descriptions

The sampling site was located inside a supersite of the Dongguan Sub-branch of Guangdong Ecological and Environmental Monitoring Center (113°47′24″E，23°01′16″N) in urban Dongguan. All the online instruments, including a scanning mobility particle sizers (SMPS, TSI model 3938), an online gas chromatography-flame ionization detector-mass spectrometer (GC-MS), a Monitor for AeRosols and Gases in Ambient Air (MARGA), an atmospheric routine monitoring system (Thermo Scientific,

42i, 43i, and 49i), a carbon analyzer (SUNSET, Model 4), and an online X-ray fluorescence spectrometer, were installed in temperature-controlled rooms (about 25°C) on the roof of a building 10 m above ground. Meteorological parameters, including wind direction and speed, relative humidity (RH), temperature (Temp), solar radiation (SR), Ultraviolet B radiation (UVB), and precipitation, were measured by the automatic meteorological station (Vaisala Company, model MAWS201 and Campbell CR 1000), which was installed on the roof of the same building. The sampling information is summarized in Table 1.

2.2. Particle number size distributions

Particle number concentration for particles with mobility diameter (D_p, similar to D_g) in the range of 4.7-63.8 nm was measured using an SMPS (TSI model 3938) combined with a differential mobility analyzer (DMA, TSI model 3085) and a condensation particle counter (CPC, TSI model 3776) at a 5-min resolution. The flow rate of the sample air and the sheath air were 1.5 and 15.0 L min^{-1}, respectively. Particle number concentration for particles in the range of 14.9-673.2 nm in mobility diameter (D_p) was measured using an SMPS (TSI model 3938) combined with a DMA (TSI model 3081) and a CPC (TSI model 3775) at a 5-min resolution. The flow rate of the sample air and the sheath air were 0.3 and 3.0 L min^{-1}, respectively. To exclude the impact of particle hygroscopic growth on the measured size distribution, ambient air was forced to pass through three total suspended particulate (TSP) cyclones, stainless steel tubes, and silica gel driers before being sampled by the SMPS. RH within the system was kept below 30%. The size-dependent diffusion losses in connecting tubes were calculated according to the method described by Yue et al. (2016). The SMPS toolkit was utilized to process the SMPS data (Wu, 2017).

2.3. Online measurements of gaseous pollutants and chemical composition of particles

An online GC-MS (airmoSCANXPERT, Chromatotec) was applied to monitor 53 VOCs species at a 1-hour resolution, including alkanes, alkenes, alkynes and aromatics. The 53 monitored VOCs were calibrated weekly using a mixed calibration gas (SCOTT, USA), and the instrument accuracy was controlled within 10%. More detailed information can refer to de Blas et al. (2011). A total of 15 VOCs species, including ethylene, acetylene, ethane, propane, isobutane, n-butane, isopentane, n-pentane, benzene, toluene, n-octane, ethylbenzene, m-xylene, p-xylene, and o-xylene, were selected in the present study, which accounted for about 90% of the total VOCs concentration. Gaseous pollutants, including SO_2, O_3, and NO_2, were measured by an atmospheric routine monitoring system (Thermo Scientific, 42i, 49i, and 42i). HONO was measured by a MARGA (ADI 2080). More detailed information can refer to Rumsey et al. (2014).

A model RT-4 Sunset semi-continuous carbon analyzer with a $PM_{2.5}$ cutoff inlet (Sunset Laboratory Inc, OR, USA) was utilized to measure OC and EC with a time resolution of 1-hour. More detailed information can refer to Bauer et al. (2009). Ten elements (K, V, Cr, Mn, Ni, Cu, Zn, As, Se, and Pb) plus Pd (for quality assurance) were semi-continuously measured by an online X-ray fluorescence spectrometer (Cooper Environmental Services, Model Xact 625i) with a $PM_{2.5}$ impactor inlet at 1-h resolution. More detailed information can refer to Furger et al. (2017).

2.4. Data analysis

2.4.1 Identification of NPF and undefined events

We used the method described by Dal Maso et al. (2005) to identify the occurrence of NPF and undefined events. In this method, synchronous increases in both N_{NUC} and

126 N_{AIT} are considered to be caused by NPF events, while an increase in either N_{NUC} or
127 N_{AIT}, but not both, is considered an undefined event, as detailed below. The criteria for
128 identifying an NPF event are: (1) at least a three-fold increase in $N_{<10nm}$ (number
129 concentration of particles with D_p < 10 nm) for at least 1 hour (the cutoff size of 10 nm
130 rather than 25 nm ($N_{10\text{-}25nm}$) was used to ensure that NPF event was originated from
131 local formation process rather than from regional transport), and (2) a synchronously at
132 least one-fold increase in N_{AIT}. The criteria for identifying the undefined event by NUC
133 based on N_{NUC} increase are: (1) at least a two-fold increase in $N_{<10nm}$, and (2) less than
134 a 15% increase in N_{AIT}. The criteria for identifying an undefined event by AIT based
135 on N_{AIT} increase are: (1) at least a 1.5-fold increase in N_{AIT}, and (2) less than a 10%
136 increase in $N_{<10nm}$. In any of the NPF or undefined events, no precipitation is allowed
137 to occur to objectively compare the intensity of NPF or undefined events in different
138 seasons. Any day not meeting the criteria of an NPF day, an undefined day by N_{NUC}
139 increase, or an undefined day by N_{AIT} increase described above was defined as a non-
140 event day.

141 **2.4.2 Estimation of formation rate and H_2SO_4 molecule concentration**

142 The formation rate (J_{dp}) describing the nucleation strength of NPF can be
143 calculated by equation (1) (Kulmala et al., 2012):

144 $$J_{dp} = \frac{dN_{dp}}{dt} + CoagS_{dp} \times N_{dp} + \frac{GR_{dp}}{\Delta dp} \times N_{dp} \quad (1)$$

145 Where N_{dp} is the particle number concentration in the size range [dp, dp+Δ dp],
146 $CoagS_{dp}$ is the particle loss rate by coagulation with other particles, and GR_{dp} is the
147 growth rate of newly formed particles. Here d_p is chosen as 4.7 nm and Δd_p as 20.3 nm,
148 corresponding to the size range of 4.7–25 nm. $CoagS_{dp}$ is calculated by equation (2)
149 (Lehtinen et al., 2007) and GR_{dp} by equation (3) (Kulmala et al., 2012) below:

$$\mathrm{CoagS_{dp}} = CS \times (\frac{dp}{0.71})^{m} \quad (2)$$

$$\mathrm{GR_{dp}} = \frac{\Delta \mathrm{GMD}}{\Delta \mathrm{t}} \quad (3)$$

In literature, the index m ranged from −1.75 to −1.5 (Kulmala et al., 2012) and −1.6 was used in the present study. The condensation sink (CS), defined as the rate at which condensable vapors condense on pre-existing particles, was calculated by equation (4) below (Lehtinen et al., 2003; Salma et al., 2011). ΔGMD is a variation of the geometric mean diameter (GMD) in the nucleation mode (4.7-25 nm).

$$\mathrm{CS} = 2\pi D \sum_{i} \beta_m(d_{p,i}) d_{p,i} N_i \quad (4)$$

Where D is the diffusion coefficient of the condensing vapor and β_m is the transition correction factor for mass flux. The variables $d_{p,i}$ and N_i are the diameter and the number concentration, respectively, of particles in size bin i. D and β_m were calculated by equations (5) and (6) below:

$$\mathrm{D} = 5.0032 \times 10^{-6} + 1.04 \times 10^{-8}\mathrm{T} + 1.64 \times 10^{-11}\mathrm{T}^2 - 1.566 \times 10^{-14}\mathrm{T}^3 \quad (5)$$

$$\beta_m = \frac{1 + \mathrm{K_n}}{1 + （\frac{4}{3\alpha} + 0.377） \mathrm{K_n} + \frac{4}{3\alpha}\mathrm{K_n^2}} \quad (6)$$

D is the diffusion coefficient ($m^2\ s^{-1}$) and T is the Kelvin temperature. T was chosen as 300.7 K in spring, 304.5 K in summer, 298.0 K in autumn, and 292.1 K in winter in the present study. α = 1 was used in the present study (Jayaratne et al., 2017). Knudsen number (K_n) was calculated by equation (7):

$$\mathrm{K_n} = \frac{2\lambda}{\mathrm{d_p}} \quad (7)$$

λ = 108 nm was used in the present study (Kulmala et al., 2012).

In addition, the molecule concentration of H_2SO_4 can be estimated by equation (8), according to the method recommended by Lu et al. (2019):

$$[H_2SO_4] = 280.05 \times UVB^{0.14} \times [SO_2]^{0.40} \quad (8)$$

Here, the unit for $[H_2SO_4]$ and $[SO_2]$ is in molecule cm^{-3}, and the unit for UVB is in W m^{-2}.

2.4.3 Weather Research and Forecasting (WRF) model and Positive matrix factorization (PMF) model

The surface wind was simulated by the WRF model (version 4.1.5) during the typical NPF events, undefined events by NUC, and undefined events by AIT. Three nested domains with horizontal resolutions of 25 km, 5 km, and 1 km, respectively, were applied, with the innermost domain covering the whole city of Dongguan. More detailed information can refer to Tao et al. (2022).

Positive matrix factorization (PMF) model version 5.0 was used to quantify the contributions of dominant potential sources to UFP in the present study. To reduce the uncertainties of PMF results, N_{UFP} (N_{NUC} and N_{AIT}), Water Soluble Inorganic Ions (WSIIs), and elements with hourly concentrations below Method Detection Limits (MDLs) were removed. In addition, 21 variables, including 3-hour average N_{UFP}, $N_{<10nm}$, $N_{10\text{-}25nm}$, N_{AIT}, estimated H_2SO_4, O_3, UVB, and chemical tracers (SO_2, NO_2, OC, EC, K, V, Cr, Mn, Ni, Cu, Zn, As, Se, and Pb) for primary combustion sources, were used as input for the PMF model. In this study, we have tested five, six, seven, and eight different sources in the PMF analysis. PMF was then run more than one hundred times with different F_{peak} values (±0.5 and ±1.0) to confirm the stabilities of the selected results. PMF results suggest a seven-factor model (F_{peak} = -0.5) provided the most physically reasonable source profiles.

3. Results and Discussion

3.1. Frequencies of the NPF and undefined days, and general characteristics of particle number concentrations

Using the criteria described in section 2.4.1, we identified 27 days having NPF events and 34 days having undefined events during the whole campaign period of a total of 105 days (Fig.1). On annual average, the frequency of NPF days was 26% in urban Dongguan, which was similar to those reported for other cities in the PRD (23%), YRD (27%), and NCP (34%) region (Chu et al., 2019; Dai et al., 2017; Deng et al., 2020; Qi et al., 2015; Wang et al., 2013c; Xiao et al., 2015; Zhang et al., 2021). Furthermore, it is worth noting that the frequencies of NPF days observed in China are similar to those observed in certain cities in India, such as in Kanpur, Hyderabad, and Pune with an average frequency of 32% (Kanawade et al., 2014; Sebastian et al., 2021; Siingh et al., 2013; 2018). Most NPF days occurred in autumn (with a frequency of 59%) and winter (33%) and only occasionally occurred in spring (4%) and summer (4%). However, if including the four NPF events occurred on rainy days in the spring and summer, the frequency of NPF days in spring and summer would be just above 10%, while the annual frequency of NPF days would also increase to 30%.

On annual average, the frequency of undefined days was 32% (34 days out of 105 days), of which 4% (4 days) was from undefined days by NUC and 28% (30 days) from undefined days by AIT. The undefined days by NUC only appeared in autumn (75%) and winter (25%), and no event in the other seasons, while the frequencies of undefined days by AIT mainly occurred in spring (47%), followed by summer (30%) and winter (17%), and least in autumn (6%) (Table 2). In addition, 5 and 7 undefined events by AIT were also observed on rainy days in spring and summer, respectively. If including these rainy-day events, the annual frequency of the undefined days would reach 44%,

which was much higher than those reported for other cities in the YRD region (4%) (Ling et al., 2019) and the NCP region (5-30%) (Cai et al., 2021; Deng et al., 2020; Wang et al., 2013a).

Annual average N_{UFP} were (18.0±16.0) $\times 10^3$ cm^{-3}, (12.6±5.3) $\times 10^3$ cm^{-3}, and (10.0±2.8) $\times 10^3$ cm^{-3}, respectively, during the NPF, undefined, and non-event days (Table 2). The ratios of N_{NUC} to N_{AIT} were 1.0±2.0, 0.6±0.8, and 0.5±0.4, respectively, during the NPF, undefined, and non-event days. The average seasonal ratio of N_{NUC} to N_{AIT} did not vary much on non-event days, with a balance of 0.5-0.7 in four seasons. In contrast, the ratios in summer during the NPF (0.6±0.5) and undefined days (0.3±0.3) were evidently lower than those in the other seasons (1.0-1.3 on NPF days and 0.6-0.8 on undefined days).

During the burst periods of NPF events, N_{NUC} was much higher than N_{AIT}, as indicated by the much higher than 1.0 ratio of N_{NUC} to N_{AIT} in all the seasons (2.0, 2.5, 6.1±2.9, and 6.6±2.3 in spring, summer, autumn, and winter, respectively). During the growth periods of NPF event, N_{NUC} decreased while N_{AIT} increased, resulting in the decreasing ratio of N_{NUC} to N_{AIT}; however, N_{NUC} was still slightly higher than N_{AIT} most of the time, as indicated by the ratio of 1.1±0.6. Thus, N_{UFP} was mainly determined by N_{NUC} during the burst period and by both N_{NUC} and N_{AIT} during the growth period of NPF events.

On the undefined days and non-event days, N_{AIT} was much higher than N_{NUC} in all four seasons. Although N_{NUC} and N_{AIT} during the undefined days were higher than those during non-event days, the ratio of N_{NUC} to N_{AIT} was similar (0.6±0.8 on undefined days and 0.5±0.4 on non-event days). In addition, the ratio of N_{NUC} to N_{AIT} was 0.5±0.3 during the undefined events by AIT, which was similar to those during the undefined events and non-event days. These results suggested N_{UFP} was mainly

244 determined by N_{AIT} during the undefined events and non-event days in four seasons. In
245 contrast, the ratio of N_{NUC} to N_{AIT} was 4.6±2.8 during the undefined events by NUC,
246 which was evidently higher than during the non-event days.

247 **3.2. Formation mechanisms of NPF events**

248 The burst periods of NPF event mainly occurred during 10:40 – 11:15 & 11:40 -
249 12:15 LT in spring (1 event), 10:15 - 11:15 LT in summer (1 event), 9:20 - 11:00 LT in
250 autumn (16 events), and 10:00 - 12:30 LT in winter (9 events) (Fig. S1 and Table S1).
251 These hours generally had high concentrations of OH radical in suburban Guangzhou
252 of the PRD region (Lu et al., 2012). The burst durations of NPF events were 1.2, 1.0,
253 1.7±0.7, and 2.5±1.0 hours in spring, summer, autumn, and winter, respectively. The
254 growth periods following the burst period of NPF events mainly occurred at 12:20 -
255 17:10 LT in spring, 11:20 - 17:50 LT in summer, 11:05 - 23:55 LT in autumn, and 12:35
256 - 23:55 LT in winter (Table S1). On seasonal average, the growth durations of NPF were
257 5.1, 6.5, 7.0±4.2, and 7.5±3.1 hours in spring, summer, autumn, and winter, respectively.

258 NPF events were mainly related to episodes of H_2SO_4, base molecules (ammonia
259 and amines), and oxidized organic molecules in urban environments in China (Cai et
260 al., 2021; Li et al., 2022; Yan et al., 2021; Yao et al., 2018). Here we used the estimated
261 molecule concentration of H_2SO_4, the measured mass concentration of atmospheric
262 oxidants (e.g., HONO and O_3, representing OH radical) and reducing gases (e.g., VOCs,
263 NO_2), and measured meteorological factors (e.g., SR, UVB) to explore the possible
264 formation mechanisms of typical NPF events in four seasons (Table S2). Generally, the
265 NPF event is always accompanied by the rapid formation of H_2SO_4 via the reaction
266 between SO_2 and OH radicals (Lu et al., 2018; Yue et al., 2010). The source of OH
267 radical mainly originated from the photolysis of HONO and O_3 in the PRD region
268 (Hofzumahaus et al., 2009; Lu et al., 2012; Tan et al., 2019). On the contrary, the sink

of OH radical was related to photochemical reactions between reducing gases (e.g., VOCs, NO_2, CO, and SO_2) and OH radical (Lu et al., 2018; Seinfeld and Pandis., 2016). The gaseous pollutants (VOCs and NO_2) would compete with SO_2 for OH radical, according to the rate constants of the reactions of OH radical with these reducing gases (Seinfeld and Pandis., 2016).

Typical NPF events were selected for the more detailed analysis below using the following selection criteria: burst duration > 1h, growth duration > 6.5h, and N_{NUC} > 35.0×10^3#cm^{-3}. Eight NPF events met the criteria, of which four were in autumn (October 29-31 and November 1), and four were in winter (December 4, 7, 8, and 27). In addition, the only NPF event in spring (May 1) and the only one in summer (August 20) were also selected for a more detailed analysis despite the fact that these two events did not meet the criteria.

Lower VOCs and NO_2 concentrations were observed during NPF burst periods, compared to those during the same hours on non-event days, on most NPF events regardless of the season, for example, at 10:00-11:00 LT (burst period, 10:40-11:15 LT and 11:40-12:15 LT) on May 1, 10:00 LT (burst period, 10:15-11:15 LT) on August 20, 9:00-10:00 LT (burst period, 9:20-11:05 LT) on October 29-31, and 9:00-14:00 LT on December 4 (burst period, 10:20-14:40 LT), December 7 (burst period, 10:50-14:40 LT), December 8 (burst period, 9:35-11:35 LT), and December 27 (burst period, 8:55-11:25 LT) (Fig.2, Fig. S2 and Fig. S3). The only two exceptions are NPF events on October 31 and November 1. On October 31, the hourly concentrations of NO_2 at 9:00-10:00 LT (burst period, 9:45-11:05 LT) were comparable, but those of VOCs were still evidently lower than those at the same hours on the non-event days in autumn (Fig. S2). On November 1, the hourly concentrations of reducing gases (VOCs and NO_2) at 9:00-10:00 LT (burst period, 9:20-10:55 LT) were comparable to those at the same hours on

294 the non-event days in autumn (Fig. 2, 3), but the hourly concentrations of H_2SO_4 (>
295 10.0×10^6 molecule cm^{-3}) during the burst period of this NPF event were 1.3 -1.5 times
296 higher than those during the typical NPF events on October 29-31. These phenomena
297 suggested that low concentrations of reducing gases (VOCs and, to a less extent, NO_2
298 on some days) and/or higher concentrations of H_2SO_4 were conducive to the occurrence
299 of NPF events.

300 In addition, the higher hourly concentrations of O_3 (67 μg m^{-3}) but lower hourly
301 concentrations of HONO (2 μg m^{-3}) at 9:00 - 10:00 LT on the NPF days than that of O_3
302 (37 μg m^{-3}) and HONO (8 μg m^{-3}) on the non-event days (Fig. 2, 3 and Fig. S2 and S3)
303 suggest that the OH radical that drove the NPF events likely originated from the
304 photolysis of O_3 rather than HONO in this urban environment (Hofzumahaus et al.,
305 2009; Lu et al., 2012). In summary, the occurrences of NPF events in urban Dongguan
306 were likely accompanied by low concentrations of reducing gases (especially VOCs
307 and NO_2) and high concentrations of H_2SO_4 and O_3.

308 Noticeably, the intensities (represented by $J_{4.7\text{-}25}$) of the typical NPF events varied
309 with season, with average $J_{4.7\text{-}25}$ values during the burst periods of NPF events being
310 much higher in summer (20.6 cm^{-3} s^{-1}) and autumn (21.5 cm^{-3} s^{-1}) than in spring (10.3
311 cm^{-3} s^{-1}) and winter (12.8 cm^{-3} s^{-1}). To further investigate the impacts of VOCs, HONO,
312 O_3, and H_2SO_4 on the intensity of NPF events, the relationships between the mass
313 concentrations of these gaseous pollutants and $J_{4.7\text{-}25}$ were discussed using the above
314 ten typical NPF events. If excluding the three outliers on November 1, December 4, and
315 December 7 (with the hourly concentration of $H_2SO_4 > 8.9\times10^6$ molecule cm^{-3}) (Fig. 4a
316 and b), a moderate positive correlation (R^2=0.65, $p<0.05$) was obtained between the
317 hourly molecule concentration of H_2SO_4 and $J_{4.7\text{-}25}$ with a slope of 3.9×10^6, and a
318 moderate positive correlation (R^2=0.45, $p<0.05$) was obtained between the hourly mass

concentration of O_3 and $J_{4.7\text{-}25}$. However, a poor correlation (R^2=0.01) was obtained between the hourly mass concentration of HONO and $J_{4.7\text{-}25}$ (Fig. S4). These results suggested the high value of $J_{4.7\text{-}25}$ was likely determined by the higher mass concentration of H_2SO_4 and O_3 in most cases of typical NPF events.

For the three exceptional days (November 1, December 4, and December 7) (Fig. 4a), a poor positive correlation (R^2=0.25, p>0.05) between the hourly molecule concentration of H_2SO_4 and $J_{4.7\text{-}25}$ was found with a much lower regression slope of 0.8×10^6 than for the other typical NPF events discussed above. However, a moderate negative correlation (R^2=0.33, p>0.05, with the data on August 20 and November 1 being excluded) was found between the hourly concentration of $J_{4.7\text{-}25}$ and VOCs (Fig. 4c). These results suggested the higher mass concentration of VOCs might suppress the intensity of NPF events, although the higher mass concentration of H_2SO_4 could trigger NPF events. In addition, a negative correlation between the mass concentration of O_3 and $J_{4.7\text{-}25}$ was found on these days (Fig. S5), likely due to the fact that the higher mass concentration of VOCs, while suppressing the intensity of NPF event, promoted the increase of O_3 mass concentration (Song et al., 2022). We thus conclude that the intensity of NPF events might be related to the higher mass concentrations of H_2SO_4 and O_3 and the lower mass concentration of VOCs in urban Dongguan.

Noticeably, only slight increases (31%±30%) in the number concentration of particles ranging from 100 to 600 nm were observed at the end of ten typical NPF events. Furthermore, the mass concentration of $PM_{2.5}$ and the dominant chemical compositions also exhibited slight increases (29%±25%) at the end of these events (Fig. S6). These increases were significantly lower than the levels (>100%) observed at the end of NPF events in the NCP region (Guo et al., 2014; Peng et al., 2021). These findings suggested that the NPF event in the PRD region resulted in a significant increase in N_{UPF}, but not

in the number and mass concentration of larger particles. This result could be attributed to the comparatively weaker intensity of NPF events and more favorable atmospheric diffusion conditions in this region, as compared to those in the NCP region (Guo et al., 2014; Kulmala et al., 2021; Peng et al., 2021). In addition, the CS/GR ratio in Dongguan ranges from 30 to 100 (Fig. S7), which is significantly lower than the range (>100) reported by Chu et al. (2019), but is roughly consistent with the range (<100) documented in Zhang et al. (2021) for urban areas in eastern China. Overall, the CS/GR ratio in Dongguan was comparable to those in the PRD and YRD regions, but lower than those in the NCP region (Chu et al., 2019; Zhang et al., 2021).

3.3. Causes of the undefined event by NUC

Undefined events by NUC were only observed in autumn (October 18, 21, and November 7) and winter (December 26). The burst periods of the undefined event by NUC were after 11:00 LT in autumn and winter (Fig. S1 and Table S3), which lagged the burst period of NPF events by around 1 hour. The burst durations of the undefined events by NUC were 2.1±0.9 and 1.8 hours in autumn and winter, respectively, similar to those of NPF events in these seasons (1.7±0.7 hours in autumn and 2.5±1.0 hours in winter). Notably, the values of $J_{4.7\text{-}25}$ were only 3.0±1.0 cm^{-3} s^{-1} and 5.5 cm^{-3} s^{-1} during the burst periods of the undefined event by NUC in autumn and winter, respectively, which were much lower than those during the burst period of NPF events in autumn (12.8±6.3 cm^{-3} s^{-1}) and winter (11.1±3.9 cm^{-3} s^{-1}).

Since there was only one undefined event by NUC in winter (December 26), the selection criteria for the typical undefined event by NUC in autumn is basically the same as the relevant parameters during the undefined event by NUC in winter. The selection criteria include $J_{4.7\text{-}25}$> 4.0 cm^{-3} s^{-1} and $N_{NUC} > 24.0\times10^3$ #cm^{-3}, which resulted in one NPF event in autumn (November 7). As a result, only two typical undefined

events by NUC were selected for more detailed analysis in autumn and winter.

The hourly concentrations of reducing gases (VOCs and NO_2), H_2SO_4, and the intensity of UVB at 11:00-14:00 LT (burst period, 11:05-14:15 LT) on November 7 and 11:00-13:00 LT (burst period, 11:35-13:25 LT) on December 26 were comparable to those during the burst period on typical NPF days in autumn and winter, respectively (Fig. 5). In addition, no obvious cloud cover was observed over Dongguan during the burst hours on November 7 and December 26 (Fig. S8), which provided an essential condition (strong intensity of UVB) for the occurrence of NPF events. These results suggested NPF events, instead of the undefined events by NUC, might have occurred on these two days. Thus, the two typical undefined events by NUC in autumn (November 7) and winter (December 26) might be the feeble NPF event to some extent. However, no evident increase in N_{AIT} was found after the burst periods, suggesting these two undefined events by NUC might be closely related with the transport of NUC from the upward wind region where the NPF event likely occurred. This hypothesis was supported by the high SO_2 mass concentration in the upwind zone (northeast of the observation site) before the burst periods (Fig. S9), where and when the NPF event probably occurred and produced a high N_{NUC}, which was then transported to the observation site in subsequent hours.

A gradually declining trend after 12:00 LT on November 7 and a sudden downward trend after 13:00 LT on December 26 in N_{NUC} were observed (Fig. 5). Meanwhile, significant decreases in SO_2 mass concentration were simultaneously observed in the upwind zone of the observation site (Fig. S9). This suggested the possible NPF event that occurred upwind of the observation site on November 7 and December 26 might have been interrupted mainly due to the significant decrease in SO_2 concentration. In addition, the significant drop in intensity of UVB after 13:00 LT on December 26 might

be another factor that interrupted the possible NPF events in the upwind zone of the observation site since UVB is an important factor affecting the formation of H_2SO_4 according to the equation (8).

3.4. Causes of the undefined event by AIT

In most cases, the burst period of undefined events by AIT was mainly found at 12:00 - 23:00 in spring (14 events) and summer (9 events), 11:00 - 14:00 in autumn (2 events), and 12:00 - 20:00 in winter (5 events) (Fig. S1 and Table S3), which was consistent with the growth period of NPF events in the corresponding season. The burst durations of undefined events by AIT were 8.7±3.8, 11.4±6.6, 1.5±0.3, and 7.2±2.2 hours in spring, summer, autumn, and winter, respectively. The burst durations of undefined events by AIT were comparable to the growth durations of NPF events in all seasons except autumn.

To further verify the above point, one typical undefined event by AIT with a long burst duration and a high N_{AIT} was selected for detailed analysis in each season of spring (May 12), summer (August 4), and winter (December 21). The undefined event by AIT in autumn was excluded because the burst durations (<2h) in autumn were much shorter than those (>10h) in the other seasons. The hourly concentrations of both VOCs and H_2SO_4 before 10:00 LT (burst period, 10:30-20:30 LT) on May 12, before 11:00 LT (burst period, 11:30-23:55 LT) on August 4, and before 11:00 LT (burst period, 11:50-22:25 LT) on December 21 were higher than those at the same hours on the NPF days of spring, summer, and winter, respectively (Fig. 6). This suggested the relatively high mass concentrations of VOCs might indeed suppress the occurrence of NPF event even under the condition of higher H_2SO_4 concentrations at the observation site.

As expected, an obvious high SO_2 mass concentration zone was found in the upwind region of the observation site before the burst period of the undefined event by

AIT (before 11:00 LT) on May 12, August 4, and December 21 (Fig. S10). In addition, no obvious cloud cover was found before 11:00 LT over Dongguan on these three days (Fig. S11). These phenomena suggested a possible NPF event might have occurred in the upwind region of the observation site on these days. High concentrations were only observed for N_{AIT} but not N_{NUC}, probably because the area where the NPF event occurred was relatively far away from the observation site. Although SO_2 mass concentration in the upwind region of the observation site gradually declined in the subsequent hours following the undefined events by AIT (Fig. S12), the duration of such event (lasted more than 10 hours) was much longer than that (<3 hours) of undefined events by NUC. This may be related to the lower wind speed over Dongguan during the burst period of undefined events by AIT, compared to that during the burst period of undefined events by NUC (Fig. S9, S10, and S12). The lower wind speed allowed new particles to stay longer in the atmosphere during the downwind transport and grow into larger particles. In general, the undefined events by AIT were likely related to the transport of new particles formed in the upwind region of the observation site where the NPF event might have occurred.

3.5. Contributions of NPF and undefined events to UFP number concentrations

As discussed in sections 3.2, 3.3, and 3.4, NPF events could cause significant increases in N_{UFP}. In addition, the undefined events by NUC and AIT were also closely related to NPF events. To quantify the contributions of NPF event, regional transport of NPF event, and primary combustion emission to N_{UFP}, PMF analysis was conducted based on key parameters of NPF events and tracers of primary combustion sources. PMF analysis identified five major source factors for UFP, including (1) NPF and undefined events, (2) traffic emission, (3) coal combustion and biomass burning, (4) ship emission, and (5) photochemical processes. The profiles of these source factors are

shown in Fig. 7.

Factor 1 (NPF and undefined events) was characterized by high concentrations of high $N_{<10nm}$, $N_{10\text{-}25nm}$, N_{AIT}, H_2SO_4, and O_3 (Fig. 7a) and accounted for 51±28%, 41±26%, and 45±27% of N_{NUC}, N_{AIT}, and N_{UFP}, respectively. As discussed in section 3.2, significant increases in both N_{NUC} and N_{AIT} and the higher molecule concentration of H_2SO_4 and the higher mass concentration of O_3 were found during the NPF and undefined days compared with those during the non-event days. Factor 2 (traffic emission) was characterized by high concentrations of N_{AIT}, NO_2, OC, EC, Cr, Mn, Cu, and Zn (Fig. 7b) (He et al., 2008; Mousavi et al., 2018) and accounted for 9±11%, 39±28%, and 28±24% of N_{NUC}, N_{AIT}, and N_{UFP}, respectively. Noticeably, the contribution of traffic emission was significantly higher to N_{AIT} than N_{NUC}. Meanwhile, the contribution of traffic emission was higher to $N_{10\text{-}25nm}$ than $N_{<10nm}$. These results suggested that traffic emission likely emitted large particles (>10 nm). Factor 3 (coal combustion and biomass burning) was characterized by high concentrations of H_2SO_4, SO_2, OC, EC, K, As, Se, and Pb (Fig. 7c) (Bi et al., 2019; Pernigotti et al., 2016; Zhang et al., 2015) and accounted for 22±20%, 2±3%, and 10±10% of N_{NUC}, N_{AIT}, and N_{UFP}, respectively. The differences were significant between coal and fuel oil emissions of NUC and AIT, despite that they are both fossil fuels. In addition, the daily variation trends of the tracers of the traffic emission (e.g., NO_2, Cr) were more similar to those of N_{NUC} and N_{AIT} than to that of the coal combustion (e.g., SO_2, Pb), especially on non-event days (Fig. S13). Thus, traffic emission might emit more NUC and AIT than coal combustion to some extent. However, significantly more NUC was linked to coal combustion than traffic emission, which may be related to the oxidation of SO_2 emitted from coal combustion forming NUC during the transportation process. Factor 4 (ship emission) was characterized by high concentrations of Ni and V (Fig. 7d) (Agrawal et

al., 2009; Hays et al., 2009) and accounted for 12±15%, 8±10%, and 9±12% of N_{NUC}, N_{AIT}, and N_{UFP}, respectively. Factor 5 (photochemical processes) was characterized by high concentrations of UVB, O_3, and H_2SO_4 (Fig. 7e) and accounted for 6±11%, 10±16%, and 8±14% of N_{NUC}, N_{AIT}, and N_{UFP}, respectively. This result suggested a weaker degree of new particle formation might have occurred under the stronger intensive of UVB conditions. Generally, N_{UFP} in urban Dongguan mainly depended on the NPF and undefined events and traffic emission.

As shown in Fig. 8, the sum of NPF and undefined events accounted for 63±22% in spring and 60±26% in summer of N_{NUC}, which were higher than those in autumn (40±25%) and winter (43±29%). In contrast, coal combustion and biomass burning contributed only 8-11% of N_{NUC} in spring and summer, much lower than those in autumn (35±19%) and winter (33±21%). Although traffic emission, ship emission, and photochemical processes had the highest contributions to N_{NUC} in winter, spring, and summer, respectively, their seasonal variations were insignificant. Regarding N_{AIT}, the sum of NPF and undefined events contributed to 51±24% and 44±25% in spring and summer, respectively, which were higher compared to those in autumn (34±23%) and winter (35±30%). The lowest contributions of ship emission (3±5%) and photochemical processes (5±9%) to N_{AIT} were observed in winter, compared to those in the other seasons (7-13%). Traffic emission contributed to 26±20% and 33±22% of N_{AIT} in spring and summer, respectively, which were lower than those in autumn (43±27%) and winter (53±30%). Coal combustion and biomass burning accounted for only 1±1% of N_{AIT} in both spring and summer, which were slightly lower than those in autumn (4±3%) and winter (3±3%).

It is worth noting that although the frequencies of NPF events were significantly higher in autumn (59%) and winter (33%) than spring (11%, including rainy days) and

summer (12%, including rainy days), the contributions of NPF and undefined events to N_{NUC} were actually higher in spring and summer than autumn and winter. Additionally, the undefined events not only significantly contributed to N_{AIT} but also appreciably contributed to N_{NUC}. Furthermore, the frequencies of the sum of NPF and undefined events in spring (81%), summer (79%), and autumn (78%) throughout the observation period were significantly higher than that in winter (55%). These results suggested that the contributions of NFP and undefined events to N_{NUC} depended on not only their frequencies but also their duration and burst intensities.

As discussed in Sections 3.2, 3.3, and 3.4, the average burst durations of NPF events in winter (2.3±1.0 h) were longer than those in autumn (1.7±0.7 h), spring (1.2 h), and summer (1 h). Meanwhile, the average burst durations of undefined events in summer (11.4±6.6 h) and spring (8.7±3.8 h) were significantly higher than those in winter (7.2±2.2 h) and autumn (1.5±0.3 h). Additionally, the burst intensities of undefined events might also be weaker in autumn and winter than spring and summer, because this was the case for the NPF events (Fig. 4a). Consequently, the higher contributions of NPF and undefined events to N_{NUC} in spring and summer than autumn and winter could be attributed to the higher frequencies, longer burst durations, and stronger burst intensities of NPF and undefined events in spring and summer.

The contributions of NPF and undefined events to N_{UFP} in spring (56±23%) and summer (51±26%) were higher than those in autumn (36±24%) and winter (37±29%). Ship emission contributed most in spring (15±15%) and photochemical processes contributed most in summer (11±19%) to N_{UFP}, compared to those in the other seasons (4-12%). Traffic emission contributed more in autumn (30±23%) and winter (41±29%) than spring (18±18%) and summer (23±19%) to N_{UFP}. The contributions of coal combustion and biomass burning to N_{UFP} were higher in autumn (16±10%) and winter

519 (13±10%) than spring (4±5%) and summer (5±5%).

520 As shown in Fig. 9, NPF and undefined events contributed significantly to N_{NUC},
521 accounting for 44-63% during 9:00-21:00 LT. This was because the burst period of NPF
522 events mostly occurred during the daytime (Table S1). It is worth noting that the
523 contributions of NPF and undefined events remained high at 39-57%, even at night.
524 This was due to the extended duration of undefined events or the growth period of NPF
525 events, which could last until the next morning. Although N_{NUC} was significantly lower
526 at night than during the daytime, the contributions of NPF and undefined events to N_{NUC}
527 were still significant compared to the other sources. Likewise, photochemical processes
528 contributed 9-19% to N_{NUC} during 9:00-18:00 LT, but negligible at night because
529 photochemical reactions only occur during the daytime. In contrast, coal combustion
530 and biomass burning (24-31%), traffic emission (11-18%), and ship emission (14-18%)
531 contributed significantly to N_{NUC} during the nighttime (21:00-6:00 LT) or early morning
532 (0:00-6:00 LT), likely due to the diurnal variation of boundary layer height and
533 characteristics of these sources activities.

534 The diurnal variations in the contributions of the five sources mentioned above to
535 N_{AIT} were consistent with the diurnal trends of their contributions to N_{NUC}. The high
536 contributions of NPF and undefined events to N_{AIT} (42-45%) were found between 6:00-
537 18:00 LT. Similarly, the contributions of photochemical processes to N_{AIT} (18-34%)
538 during 9:00-18:00 LT were much higher than that at night (0%). In contrast, high
539 contributions of traffic emission (46-57%) and ship emission (7-12%) to N_{AIT} occurred
540 during nighttime (21:00-6:00 LT) or early morning (0:00-6:00 LT). The contribution of
541 coal combustion and biomass burning to N_{AIT} during the nighttime (3-4%) was only
542 slightly higher than that during the daytime (1-2%).

543 As a result, high contributions of NPF and undefined events (46-51%) and

photochemical processes (1-27%) to N_{UFP} occurred during the daytime, while those of traffic emission (34-44%), coal combustion and biomass burning (9-14%), and ship emission (7-14%) to N_{UFP} occurred during the nighttime. In general, N_{UFP} was determined by NPF and undefined events and photochemical processes during the daytime, while N_{UFP} was controlled by traffic emission, coal combustion and biomass burning, and ship emission during the nighttime.

4. Conclusions

This study investigated the occurrence frequencies of the NPF and undefined days, explored possible formation mechanisms of NPF events and undefined events by NUC and AIT, and quantified the contributions of NPF and undefined events to N_{UFP} in different seasons in urban Dongguan of South China. The NPF events in this city were mainly caused by low concentrations of reducing gases (especially VOCs and NO_2) and high concentrations of O_3 and H_2SO_4. The undefined events by NUC and AIT were mainly caused by regional transport of NPF from the upwind region where NPF events likely occurred.

NPF and undefined events and traffic emission were the dominant sources of N_{UFP}. Besides the NPF and undefined events, coal combustion and biomass burning was the second largest contributor to N_{NUC}, while traffic emission was the second largest contributor to N_{AIT}. Considering that the undefined event by NUC and AIT were both related to NPF events in the upwind region, further controlling coal combustion and traffic emission would be an effective way to alleviate the effects of UFP on haze formation and human health in the PRD region. Future studies in this region should measure H_2SO_4 and OH radicals, especially in the industrial zone where large amounts of SO_2 are emitted, to confirm the potential formation mechanisms of NPF and undefined events revealed in the present study.

Data availability. Data used in this study are available from Jun Tao (taojun@jnu.edu.cn).

Competing interests. The authors declare that they have no conflict of interest.

Acknowledgments

This study was supported by the National Natural Science Foundation of China (No. 41875160).

References

Agrawal, H., Eden, R., Zhang, X., Fine, P.M., Katzenstein, A., Miller, J.W., et al., 2009. Primary particulate matter from ocean-going engines in the southern California Air Basin. Environ. Sci. Technol. 43, 5398-5402.

Bauer, J.J., Yu, X.Y., Cary, R., Laulainen, N., Berkowitz, C., 2009. Characterization of the sunset semi-continuous carbon aerosol analyzer. J. Air Waste Manag Assoc. 59, 826-833.

Bi, X., Dai, Q., Wu, J., Zhang, Q., Zhang, W., Luo, R., et al., 2019. Characteristics of the main primary source profiles of particulate matter across China from 1987 to 2017. Atmos. Chem. Phys. 19, 3223-3243.

Brines, M., Dall'Osto, M., Beddows, D.C.S., Harrison, R.M., Gómez-Moreno, F., Núñez, L., et al., 2015. Traffic and nucleation events as main sources of ultrafine particles in high-insolation developed world cities. Atmos. Chem. Phys. 15, 5929-5945.

Buenrostro Mazon, S., Riipinen, I., Schultz, D.M., Valtanen, M., Dal Maso, M., Sogacheva, L., et al., 2009. Classifying previously undefined days from eleven years of aerosol-particle-size distribution data from the SMEAR II station, Hyytiälä, Finland. Atmos. Chem. Phys. 9, 667-676.

Cai, R., Yan, C., Yang, D., Yin, R., Lu, Y., Deng, C., et al., 2021. Sulfuric acid–amine nucleation in urban Beijing. Atmos. Chem. Phys. 21, 2457-2468.

Chu, B., Kerminen, V.M., Bianchi, F., Yan, C., Petäjä, T., Kulmala, M., 2019. Atmospheric new particle formation in China. Atmos. Chem. Phys. 19, 115-138.

Dai, L., Wang, H., Zhou, L., An, J., Tang, L., Lu, C., et al., 2017. Regional and local new particle formation events observed in the Yangtze River Delta region, China. J. Geophys. Res. 122(4), 2389-2402.

de Blas, M., Navazo, M., Alonso, L., Durana, N., Iza, J., 2011. Automatic on-line monitoring of atmospheric volatile organic compounds: gas chromatography-mass spectrometry and gas chromatography-flame ionization detection as complementary systems. Sci. Total Environ. 409, 5459-69.

Deng, C., Fu, Y., Dada, L., Yan, C., Cai, R., Yang, D., et al., 2020. Seasonal characteristics of New Particle Formation and growth in urban Beijing. Environ. Sci. Technol. 54, 8547-8557.

Furger, M., Minguillón, M.C., Yadav, V., Slowik, J.G., Hüglin, C., Fröhlich, R., et al., 2017. Elemental composition of ambient aerosols measured with high temporal resolution using an online XRF spectrometer. Atmos. Meas. Tech. 10, 2061-2076.

Gong, Y., Hu, M., Cheng, Y., Su, H., Yue, D.L., Liu, F., et al., 2010. Competition of coagulation sink and source rate: New particle formation in the Pearl River Delta of China. Atmos. Environ. 44, 3278-3285.

Guo, S., Hu, M., Zamora, M.L., Peng, J., Shang, D., Zheng, J., et al., 2014. Elucidating severe urban

haze formation in China. Proc. Natl. Acad. Sci. U. S. A. 111 (49), 17373–17378.
Hays, M.D., Beck, L., Barfield, P., Willis, R.D., Landis, M.S., Stevens, R.K., et al., 2009. Physical and Chemical Characterization of Residual Oil-Fired Power Plant Emissions. Energy. Fuels. 23, 2544-2551.
He, L.Y., Hu, M., Zhang, Y.H., Huang, X.F., Yao, T.T., 2008. Fine Particle Emissions from On-Road Vehicles in the Zhujiang Tunnel, China. Environ. Sci. Technol. 42: 4461-4466.
Hofzumahaus, A., Rohrer, F., Lu, K., Bohn, B., Brauers, T., Chang, C.C., et al., 2009. Amplified Trace Gas Removal in the Troposphere. Science. 324, 1702-1704.
Huang, X., Ge, X., Liu, D., Tong, L., Nie, D., Shen, F., et al., 2022. Atmospheric particle number size distribution and size-dependent formation rate and growth rate of neutral and charged new particles at a coastal site of eastern China. Atmos. Environ. 270, 118899.
Huang, X., Wang, C., Peng, J., He, L., Cao, L., Zhu, Q., et al., 2017. Characterization of particle number size distribution and new particle formation in Southern China. J Environ Sci (China). 51, 342-351.
Jayaratne, R., Pushpawela, B., He, C., Li, H., Gao, J., Chai, F., et al., 2017. Observations of particles at their formation sizes in Beijing, China. Atmos. Chem. Phys. 171, 8825-8835.
Junkermann, W., Hacker, J.M., 2018. Ultrafine Particles in the Lower Troposphere: Major Sources, Invisible Plumes, and Meteorological Transport Processes. Bull Am Meteorol Soc. 99, 2587-2602.
Kanawade, V.P., Tripathi, S.N., Siingh, D., Gautam, A.S., Srivastava, A.K., Kamra, A.K., et al., 2014. Observations of new particle formation at two distinct Indian subcontinental urban locations. Atmos. Environ. 96, 370-379.
Kulmala, M., Cai, R., Stolzenburg, D., Zhou, Y,. Dada, L., Guo, Y., et al., 2022. The contribution of new particle formation and subsequent growth to haze formation. Environ Sci Atmos. 2, 352-361.
Kulmala, M., Dada, L., Daellenbach, K., Yan, C., Stolzenburg, D., Kontkanen, J., et al., 2021. Is reducing new particle formation a plausible solution to mitigate particulate air pollution in Beijing and other Chinese megacities? Faraday Discuss. 226, 334-347.
Kulmala, M., Petäjä, T., Nieminen, T., Sipilä, M., Manninen, H.E., Lehtipalo, K., et al., 2012. Measurement of the nucleation of atmospheric aerosol particles. Nat. Protoc. 7, 1651-1667.
Lehtinen, K.E.J., Korhonen, H., Dal, Maso.M., Kulmala, M., 2003. On the concept of condensation sink diameter. Boreal Environ. Res. 8, 405-411.
Lehtinen, K.E.J., Dal, Maso.M., Kulmala, M., Kerminen, V.M., 2007. Estimating nucleation rates from apparent particle formation rates and vice versa: Revised formulation of the Kerminen–Kulmala equation. J. Aerosol Sci. 38, 988-994.
Li, X., Li, Y., Cai, R., Yan, C., Qiao, X., Guo, Y., et al.,2022. Insufficient Condensable Organic Vapors Lead to Slow Growth of New Particles in an Urban Environment. Environ. Sci. Technol. 56(14), 9936-9946.
Liang, C.S., Yue, D.L., Wu, H., Shi, J.S., He, K.B., 2021. Source apportionment of atmospheric particle number concentrations with wide size range by nonnegative matrix factorization (NMF). Environ. Pollut. 289, 117846.
Ling, Y., Wang, Y., Duan, J., Xie, X., Liu, Y., Peng, Y., et al., 2019. Long-term aerosol size distributions and the potential role of volatile organic compounds (VOCs) in new particle formation events in Shanghai. Atmos. Environ. 202, 345-356.
Lin, L.Z., Gao, M., Xiao, X., Knibbs, L.D., Morawska, L., Dharmage, S.C., et al., 2021. Ultrafine particles, blood pressure and adult hypertension: a population-based survey in Northeast China. Environ. Res. Lett. 16(9), 094041.

Liu, S., Hu, M., Wu, Z., Wehner, B., Wiedensohler, A., Cheng, Y., 2008. Aerosol number size distribution and new particle formation at a rural/coastal site in Pearl River Delta (PRD) of China. Atmos. Environ. 42, 6275-6283.

Liu, Z.R., Hu, B., Liu, Q., Sun, Y., Wang, Y.S., 2014. Source apportionment of urban fine particle number concentration during summertime in Beijing. Atmos. Environ. 96, 359-369.

Lu, K.D., Rohrer, F., Holland, F., Fuchs, H., Bohn, B., Brauers, T., et al., 2012. Observation and modelling of OH and HO_2 concentrations in the Pearl River Delta 2006: a missing OH source in a VOC rich atmosphere. Atmos. Chem. Phys. 12, 1541-1569.

Lu, K., Guo, S., Tan, Z., Wang, H., Shang, D., Liu, Y., et al., 2018. Exploring atmospheric free-radical chemistry in China: the self-cleansing capacity and the formation of secondary air pollution. Natl. Sci. Rev. 6, 579-594.

Lu, Y., Yan, C., Fu, Y., Chen, Y., Liu, Y., Yang, G., et al., 2019. A proxy for atmospheric daytime gaseous sulfuric acid concentration in urban Beijing. Atmos. Chem. Phys. 19, 1971-1983.

Mejía, J.F., Morawska, L., Mengersen, K., 2008. Spatial variation in particle number size distributions in a large metropolitan area. Atmos. Chem. Phys. 8, 1127-1138.

Mishra, S., Tripathi, S.N., Kanawade, V.P., Haslett, S.L., Dada, L., Ciarelli, G., et al., 2023. Rapid night-time nanoparticle growth in Delhi driven by biomass-burning emissions. Nat. Geosci. 16, 224–230.

Mousavi, A., Sowlat, M.H., Sioutas, C., 2018. Diurnal and seasonal trends and source apportionment of redox-active metals in Los Angeles using a novel online metal monitor and Positive Matrix Factorization (PMF). Atmos. Environ. 174, 15-24.

Németh, Z., Rosati, B., Zíková, N., Salma, I., Bozó, L., Dameto, D.E.C., et al., 2018. Comparison of atmospheric new particle formation events in three Central European cities. Atmos. Environ. 178, 191-197.

Peng, J., Hu, M., Shang, D., Wu, Z., Du, Z., Tan, T., et al., 2021. Explosive Secondary Aerosol Formation during Severe Haze in the North China Plain. Environ. Sci. Technol. 55, 2189–2207.

Pernigotti, D., Belis, C.A., Spanò, L., 2016. SPECIEUROPE: The European data base for PM source profiles. Atmospheric Pollut. Res. 7, 307-314.

Qi, X.M., Ding, A.J., Nie, W., Petäjä, T., Kerminen, V.M., Herrmann, E., et al., 2015. Aerosol size distribution and new particle formation in the western Yangtze River Delta of China: 2 years of measurements at the SORPES station. Atmos. Chem. Phys. 15, 12445-12464.

Rivas, I., Beddows, D.C.S., Amato, F., Green, D.C., Jarvi, L., Hueglin, C., et al., 2020. Source apportionment of particle number size distribution in urban background and traffic stations in four European cities. Environ Int. 135, 105345.

Rumsey, I.C., Cowen, K.A., Walker, J.T., Kelly, T.J., Hanft, E.A., Mishoe, K., et al., 2014. An assessment of the performance of the Monitor for AeRosols and GAses in ambient air (MARGA): a semi-continuous method for soluble compounds. Atmos. Chem. Phys. 14, 5639-5658.

Salma, I., Borsós, T., Weidinger, T., Aalto, P., Hussein, T., Dal, Maso. M., et al., 2011. Production, growth and properties of ultrafine atmospheric aerosol particles in an urban environment. Atmos. Chem. Phys. 11, 1339-1353.

Schraufnagel, D.E., 2020. The health effects of ultrafine particles. Exp Mol Med. 52(3), 311-317.

Sebastian, M., Kanawade, V.P., Pierce, J.R., 2021. Observation of sub-3nm particles and new particle formation at an urban location in India. Atmos. Environ. 256, 118460.

Seinfeld, J.H., and Pandis, S.N., 2016. Atmospheric Chemistry and Physics: From Air Pollution to Climate Change.

Shang, D., Hu, M., Tang, L., Fang, X., Liu, Y., Wu, Y., et al., 2023. Significant effects of transport on nanoparticles during new particle formation events in the atmosphere of Beijing. Particuology. https://doi.org/10.1016/j.partic.2022.12.006.

Siingh, D., Gautam, A., Kamra, A., Komsaare, K.J., 2013. Nucleation events for the formation of charged aerosol particles at a tropical station—preliminary results. Atmos. Res. 132, 239-252.

Siingh, D., Gautam, A.S., Buchunde, P., Kamra, A.K., 2018. Classification of the new particle formation events observed at a tropical site, Pune, India. Atmos. Environ. 190, 10-22.

Song, K., Liu, R., Wang, Y., Liu, T., Wei, L., Wu, Y., et al., 2022. Observation-based analysis of ozone production sensitivity for two persistent ozone episodes in Guangdong, China. Atmos. Chem. Phys. 22, 8403-8416.

Sowlat, M.H., Hasheminassab, S., Sioutas, C., 2016. Source apportionment of ambient particle number concentrations in central Los Angeles using positive matrix factorization (PMF). Atmos. Chem. Phys. 16, 4849-4866.

Tan, H.B., Yin, Y., Li, F., Liu, X.T., Chan, P.W., Deng T., et al., 2016. Measurements of particle number size distributions and new particle formations events during winter in the Pearl River Delta region, China. J. Trop. Meteorol. 22 (2), 191-199.

Tang, L., Shang, D., Fang, X., Wu, Z., Qiu, Y., Chen, S., et al., 2021. More Significant Impacts From New Particle Formation on Haze Formation During COVID-19 Lockdown. Geophys. Res. Lett. 48(8) (e2020GL091591).

Tan, Z., Lu, K., Hofzumahaus, A., Fuchs, H., Bohn, B., Holland, F., et al., 2019. Experimental budgets of OH, HO2, and RO2 radicals and implications for ozone formation in the Pearl River Delta in China 2014. Atmos. Chem. Phys. 19, 7129-7150.

Tao, J., Zhang, Z., Zhang, L., Li, J., Wu, Y., Pei, C., et al., 2022. Quantifying the relative contributions of aqueous phase and photochemical processes to water-soluble organic carbon formation in winter in a megacity of South China. Chemosphere. 300, 134598.

Varanda Rizzo, L., Roldin P., Brito J., Backman J., Swietlicki E., Krejci R., et al., 2018. Multi-year statistical and modeling analysis of submicrometer aerosol number size distributions at a rain forest site in Amazonia. Atmos. Chem. Phys. 18, 10255-10274.

Wang, Z.B., Hu M., Sun JY., Wu ZJ., Yue DL., Shen XJ., et al., 2013a. Characteristics of regional new particle formation in urban and regional background environments in the North China Plain. Atmos. Chem. Phys. 13, 12495-12506.

Wang, Z.B., Hu, M., Wu, Z.J., Yue, D.L., He, L.Y., Huang, X.F., et al., 2013b. Long-term measurements of particle number size distributions and the relationships with air mass history and source apportionment in the summer of Beijing. Atmos. Chem. Phys. 13, 10159-10170.

Wang, Z.B., Hu, M., Yue, D.L., He, L.Y., Huang, X.F., Yang, Q., et al., 2013c. New particle formation in the presence of a strong biomass burning episode at a downwind rural site in PRD, China. Tellus B. 65, 19965.

Wu, C., 2017. SMPS Toolkit. Zenodo. https://doi.org/10.5281/zenodo.1215284.

Wu, H., Li, Z., Jiang, M., Liang, C., Zhang, D., Wu, T., et al., 2021. Contributions of traffic emissions and new particle formation to the ultrafine particle size distribution in the megacity of Beijing. Atmos. Environ. 262, 118652.

Xiao, S., Wang, M.Y., Yao, L., Kulmala, M., Zhou, B., Yang, X., et al., 2015. Strong atmospheric new particle formation in winter in urban Shanghai, China. Atmos. Chem. Phys. 15, 1769-1781.

Yadav, S.K., Kompalli, S.K., Gurjar, B.R., Mishra, R.K., 2021. Aerosol number concentrations and new

particle formation events over a polluted megacity during the COVID-19 lockdown. Atmos. Environ. 259, 118526.

Yan, C., Yin, R., Lu, Y., Dada, L., Yang, D., Fu, Y., et al., 2021. The Synergistic Role of Sulfuric Acid, Bases, and Oxidized Organics Governing New-Particle Formation in Beijing. Geophys. Res. Lett. 48(7) (e2020GL091944).

Yao, L., Garmash, O., Bianchi, F., Zheng, J., Yan, C., Kontkanen, J., et al., 2018. Atmospheric new particle formation from sulfuric acid and amines in a Chinese megacity. Science. 361, 278-281.

Yue, D.L., Hu, M., Zhang, R.Y., Wang, Z.B., Zheng, J., Wu, Z.J., et al., 2010. The roles of sulfuric acid in new particle formation and growth in the mega-city of Beijing. Atmos. Chem. Phys. 10, 4953-4960.

Yue, D.L., Hu, M., Wang, Z.B., Wen, M.T., Guo, S., Zhong, L.J., et al., 2013. Comparison of particle number size distributions and new particle formation between the urban and rural sites in the PRD region, China. Atmos. Environ. 76, 181-188.

Yue, D.L., Zhong, L., Zhang, T., Shen, J., Yuan, L., Ye, S., et al., 2016. Particle Growth and Variation of Cloud Condensation Nucleus Activity on Polluted Days with New Particle Formation: A Case Study for Regional Air Pollution in the PRD Region, China. Aerosol Air Qual. Res. 16, 323-335.

Zhang, D., Li, Z., Wu, H., Wu, T., Ren, R., Cai, Z., et al., 2022. Analysis of aerosol particle number size distribution and source attribution at three megacities in China. Atmos. Environ. 279, 114-119.

Zhang, Q., Jia, S., Yang, L., Krishnan, P., Zhou, S., Shao, M., et al., 2021. New particle formation (NPF) events in China urban clusters given by sever composite pollution background. Chemosphere. 262, 127842.

Zhang, X., Zhang, Y., Sun, J., Zheng, X., Li, G., Deng, Z., 2017. Characterization of particle number size distribution and new particle formation in an urban environment in Lanzhou, China. J. Aerosol Sci. 103, 53-66.

Zhang, Z., Gao, J., Engling, G., Tao, J., Chai, F., Zhang, L., et al., 2015. Characteristics and applications of size-segregated biomass burning tracers in China's Pearl River Delta region. Atmos. Environ. 102, 290-301.

Zhao, S., Yu, Y., Li, J., Yin, D., Qi, S., Qin, D., 2021. Response of particle number concentrations to the clean air action plan: lessons from the first long-term aerosol measurements in a typical urban valley in western China. Atmos. Chem. Phys. 21, 14959-14981.

Highlights:

- High frequencies of NPF and undefined days were found in autumn.
- The NPF event was accompanied with low concentrations of reducing gases.
- The undefined event was mainly caused by upwind regional transport of NPF.
- NPF event and traffic emission were the dominant sources of UFP.

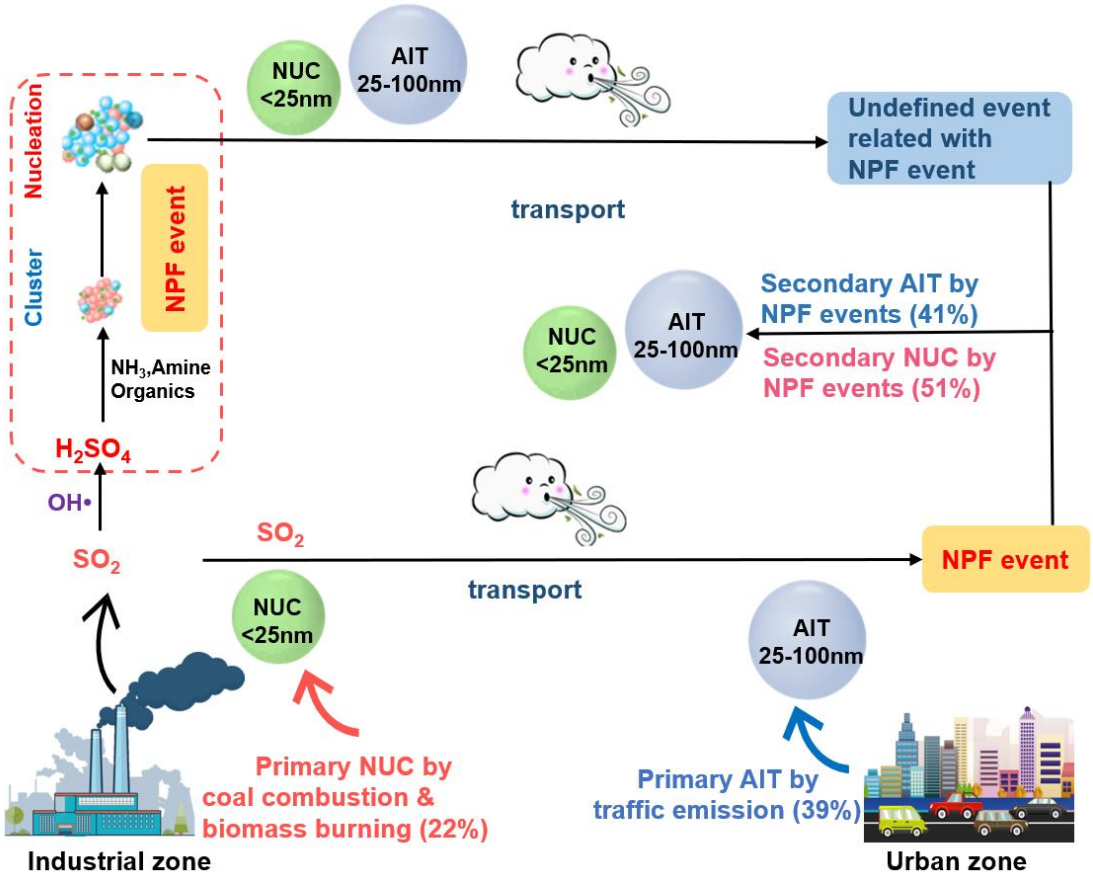
NUC
<25nm
AIT
25-100nm
Undefined event
related with
NPF event
transport
Nucleation
Cluster
NPF event
NH3,Amine
Organics
H2SO4
OH•
SO2
Secondary AIT by
NPF events (41%)
Secondary NUC by
NPF events (51%)
NUC
<25nm
AIT
25-100nm
SO2
transport
NPF event
NUC
<25nm
AIT
25-100nm
Primary NUC by
coal combustion &
biomass burning (22%)
Primary AIT by
traffic emission (39%)
Industrial zone
Urban zone

Table 1 Summary of the sAITling information

Date	SAITle type	Instruments	SAITle duration
23 April–19 May 2019 (spring)	Particle number size distribution (4.7-63.8 nm)	SMPS, TSI 3938 (DMA, TSI 3085 and CPC, TSI 3776)	5min
	Particle number size distribution (14.9-673.2 nm)	SMPS, TSI 3938 (DMA, TSI 3081 and CPC, TSI 3775)	5min
28 July–21 August 2019 (summer)	SO_2	Thermo 43i	1h
	O_3	Thermo 49i	1h
	VOCs	airmoSCANXPERT, Chromatotec	1h
18 October–13 November 2019 (autumn)	NO_2	Thermo 42i	1h
	UVB/SR	CAITbell CR 1000	1h
	RH/T/Rain	Vaisala Company, model MAWS201	1h
4–30 December 2019 (winter)	OC/EC	SUNSET Model 4	1h
	Elements	Cooper Environmental Services, Model Xact® 625i	1h
	HONO	MAGAR ADI2080	1h

The data is missing on August 10.

Table 2 Summary of number concentrations and geometric mean diameters (GMDs) in the different size modes

Period	Size mode	Annual			Spring			Summer			Autumn			Winter		
		N	Number (10^3 cm^{-3})	GMD (nm)	N	Number (10^3 cm^{-3})	GMD (nm)	N	Number (10^3 cm^{-3})	GMD (nm)	N	Number (10^3 cm^{-3})	GMD (nm)	N	Number (10^3 cm^{-3})	GMD (nm)
NPF Undefined Non-NPF	UFP 4.7-100nm	82	14.1±11.2	42±21	17	13.3±5.3	43±19	11	14.1±6.5	56±18	27	14.2±14.0	40±23	27	14.6±11.1	39±20
	NUC 4.7-25nm		6.1±9.3 43±19%			4.9±2.9 37±16%			3.8±3.6 27±13%			6.8±11.3 48±20%			6.7±9.8 46±20%	
	AIT 25-100nm		8.0±4.5 57±19%			8.4±4.1 63±16%			10.3±4.2 73±13%			7.4±5.1 52±20%			7.9±4.0 54±20%	
NPF	UFP 4.7-100nm	27	18.0±16.0	37±22	1	14.5±11.2	25±7	1	21.2±13.6	37±20	16	17.9±17.4	40±23	9	20.6±16.5	33±19
	NUC 4.7-25nm		9.2±13.5 51±22%			7.4±6.1 51±11%			8.1±8.3 38±13%			9.0±14.3 50±22%			11.6±15.2 56±24%	
	AIT 25-100nm		8.8±5.9 49±22%			7.1±6.1 49±11%			13.2±7.4 62±13%			8.9±6.2 50±22%			9.0±5.6 44±24%	
Undefined	UFP 4.7-100nm	4[a] 30[b]	12.6±5.3	49±21	14[b]	13.4±4.9	44±19	9[b]	13.6±4.9	57±17	3[a] 2[b]	10.4±5.6	39±23	1[a] 5[b]	13.5±5.8	39±20
	NUC 4.7-25nm		4.5±4.0 36±17%			4.8±2.6 35±16%			3.4±2.5 25±12%			4.7±5.3 45±18%			5.1±3.8 38±18%	
	AIT 25-100nm		8.1±3.6 64±17%			8.6±4.0 65±16%			10.2±3.7 75±12%			5.7±2.2 55±18%			8.4±3.8 62±18%	
Non-NPF	UFP 4.7-100nm	21	10.0±2.8	44±20	2	11.9±2.6	43±16	1	11.5±2.7	53±17	6	8.4±2.1	43±22	12	10.4±2.8	44±19
	NUC 4.7-25nm		3.5±1.8 35±13%			4.8±1.8 40±14%			3.7±2.1 32±10%			2.8±1.2 34±11%			3.6±2.0 34±14%	
	AIT 25-100nm		6.5±2.0 65±13%			7.1±2.1 60±14%			7.8±1.3 68±10%			5.6±1.7 66±11%			6.8±1.9 66±14%	
Rain	UFP 4.7-100nm	23	13.6±6.6	40±18	10	14.1±6.5	34±15	13	12.9±6.8	40±16	0			0		
	NUC 4.7-25nm		5.5±4.2 41±15%			6.2±3.7 44±14%			5.1±4.3 40±15%							
	AIT 25-100nm		8.1±4.2 59±15%			7.9±4.7 56±14%			7.8±4.1 60±15%							

Note: a) undefined event by NUC; b) undefined event by AIT.

List of Figures

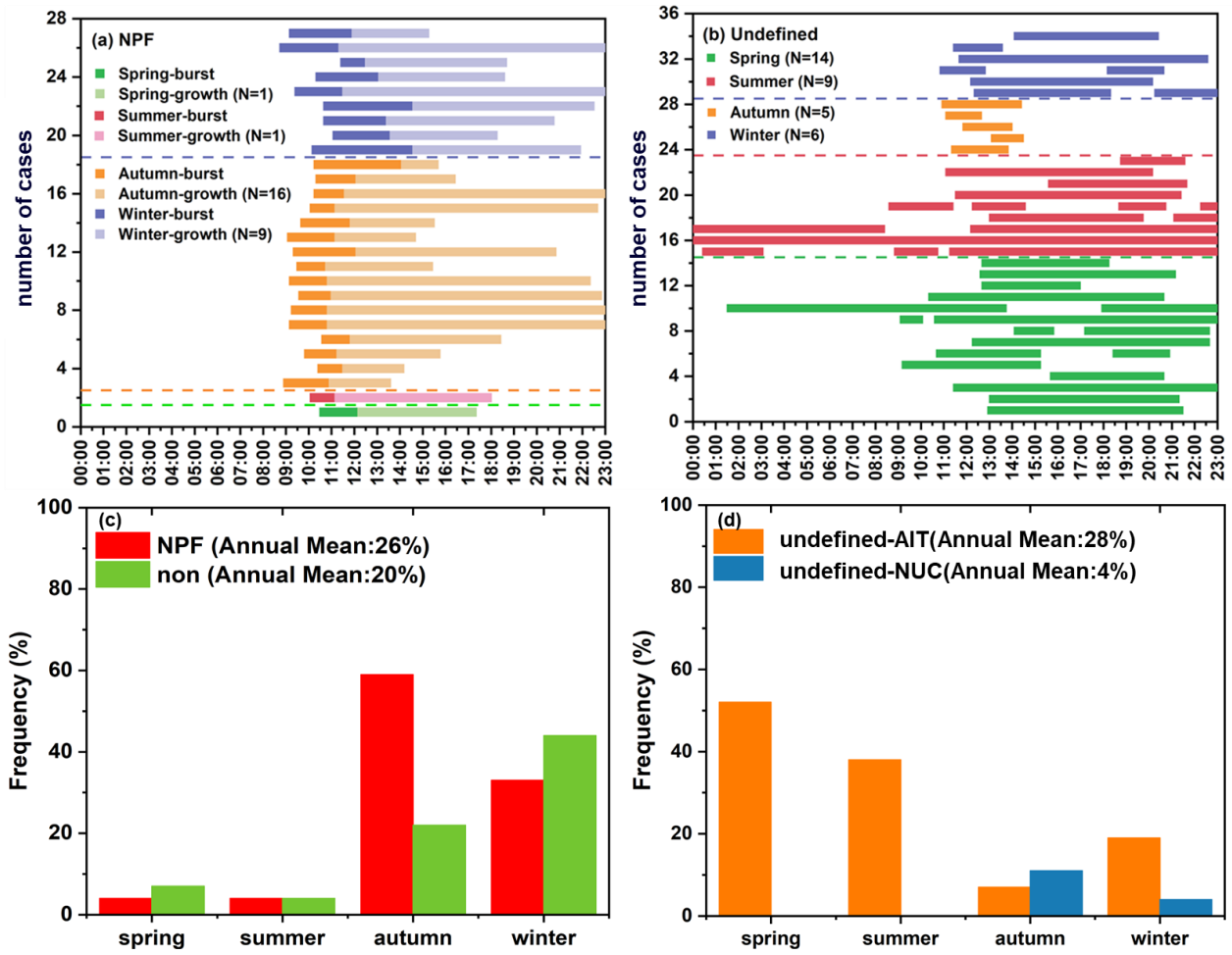
(a) NPF
Spring-burst
Spring-growth (N=1)
Summer-burst
Summer-growth (N=1)
Autumn-burst
Autumn-growth (N=16)
Winter-burst
Winter-growth (N=9)
number of cases
(b) Undefined
Spring (N=14)
Summer (N=9)
Autumn (N=5)
Winter (N=6)
number of cases
(c)
NPF (Annual Mean:26%)
non (Annual Mean:20%)
Frequency (%)
spring
summer
autumn
winter
(d)
undefined-AIT(Annual Mean:28%)
undefined-NUC(Annual Mean:4%)
Frequency (%)
spring
summer
autumn
winter

Fig.1

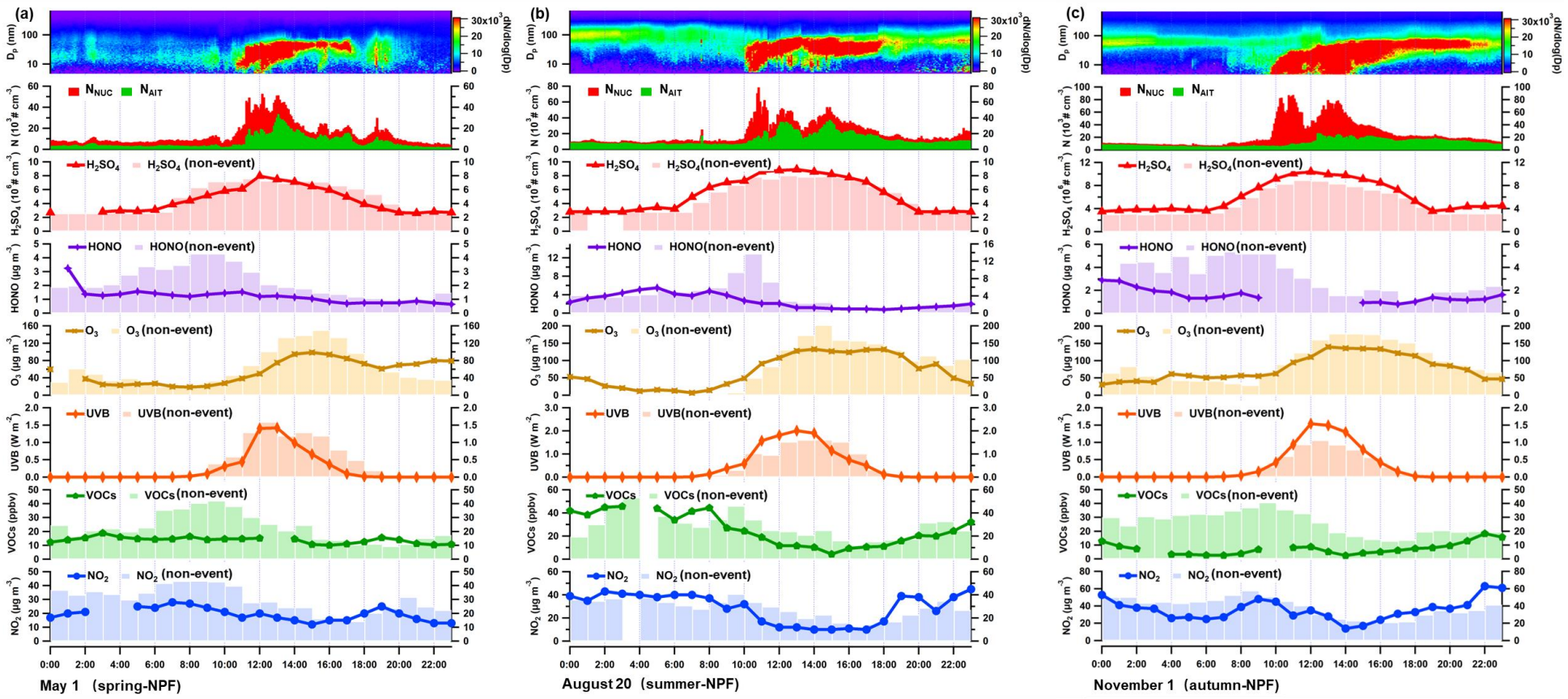
(a)
(b)
(c)
D_p (nm)
dN/dlog(Dp)
N_{NUC}
N_{AIT}
N (10^3# cm^{-3})
H_2SO_4
H_2SO_4 (non-event)
H_2SO_4 (10^6# cm^{-3})
HONO
HONO(non-event)
HONO (μg m^{-3})
O_3
O_3 (non-event)
O_3 (μg m^{-3})
UVB
UVB(non-event)
UVB (W m^{-2})
VOCs
VOCs(non-event)
VOCs (ppbv)
NO_2
NO_2 (non-event)
NO_2 (μg m^{-3})
0:00 2:00 4:00 6:00 8:00 10:00 12:00 14:00 16:00 18:00 20:00 22:00
May 1 (spring-NPF)
August 20 (summer-NPF)
November 1 (autumn-NPF)

Fig.2

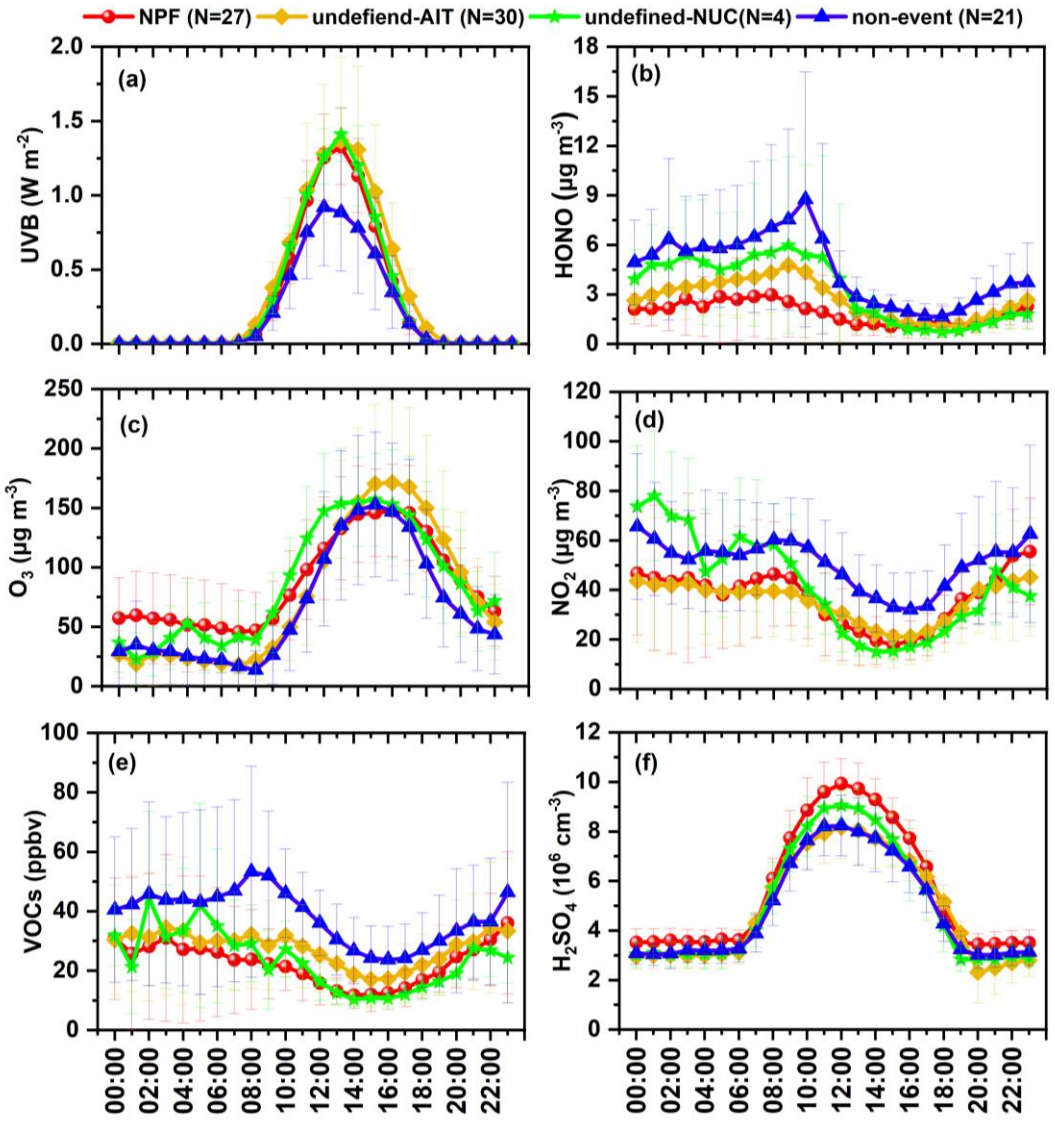
NPF (N=27)
undefiend-AIT (N=30)
undefined-NUC(N=4)
non-event (N=21)
(a)
UVB (W m-2)
(b)
HONO (μg m-3)
(c)
O3 (μg m-3)
(d)
NO2 (μg m-3)
(e)
VOCs (ppbv)
(f)
H2SO4 (10^6 cm-3)
00:00
02:00
04:00
06:00
08:00
10:00
12:00
14:00
16:00
18:00
20:00
22:00

Fig.3

Fig.4

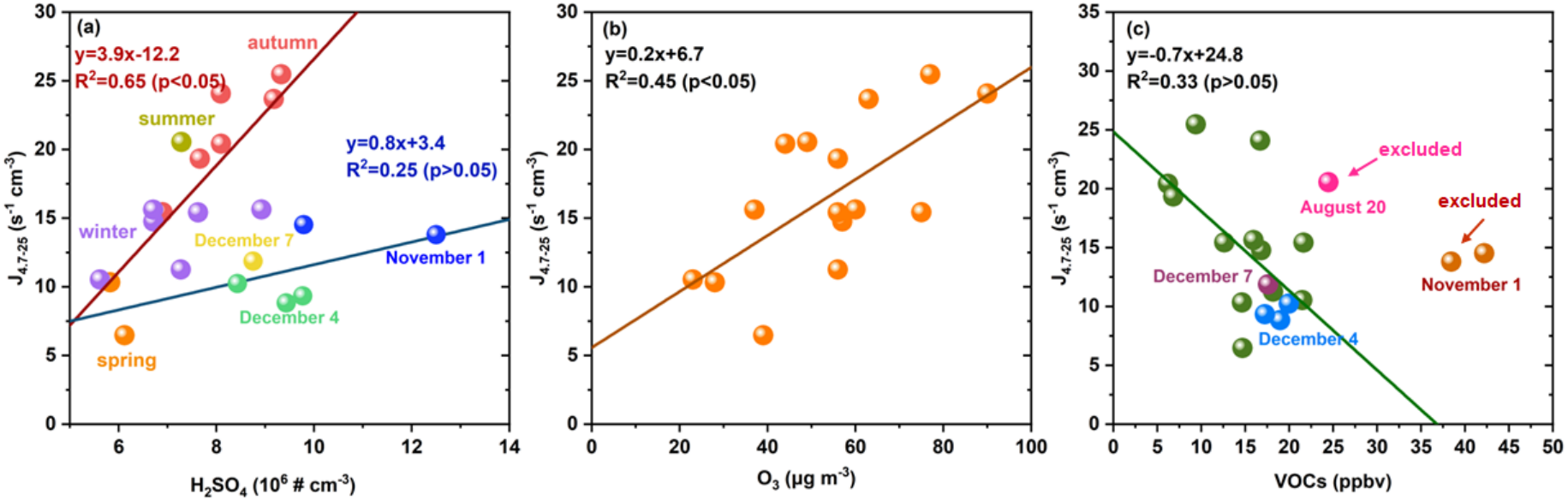
(a)
y=3.9x-12.2
R²=0.65 (p<0.05)
autumn
summer
y=0.8x+3.4
R²=0.25 (p>0.05)
winter
December 7
November 1
December 4
spring
J4.7-25 (s-1 cm-3)
H2SO4 (10⁶ # cm-3)
(b)
y=0.2x+6.7
R²=0.45 (p<0.05)
O3 (μg m-3)
(c)
y=-0.7x+24.8
R²=0.33 (p>0.05)
excluded
August 20
excluded
December 7
November 1
December 4
VOCs (ppbv)

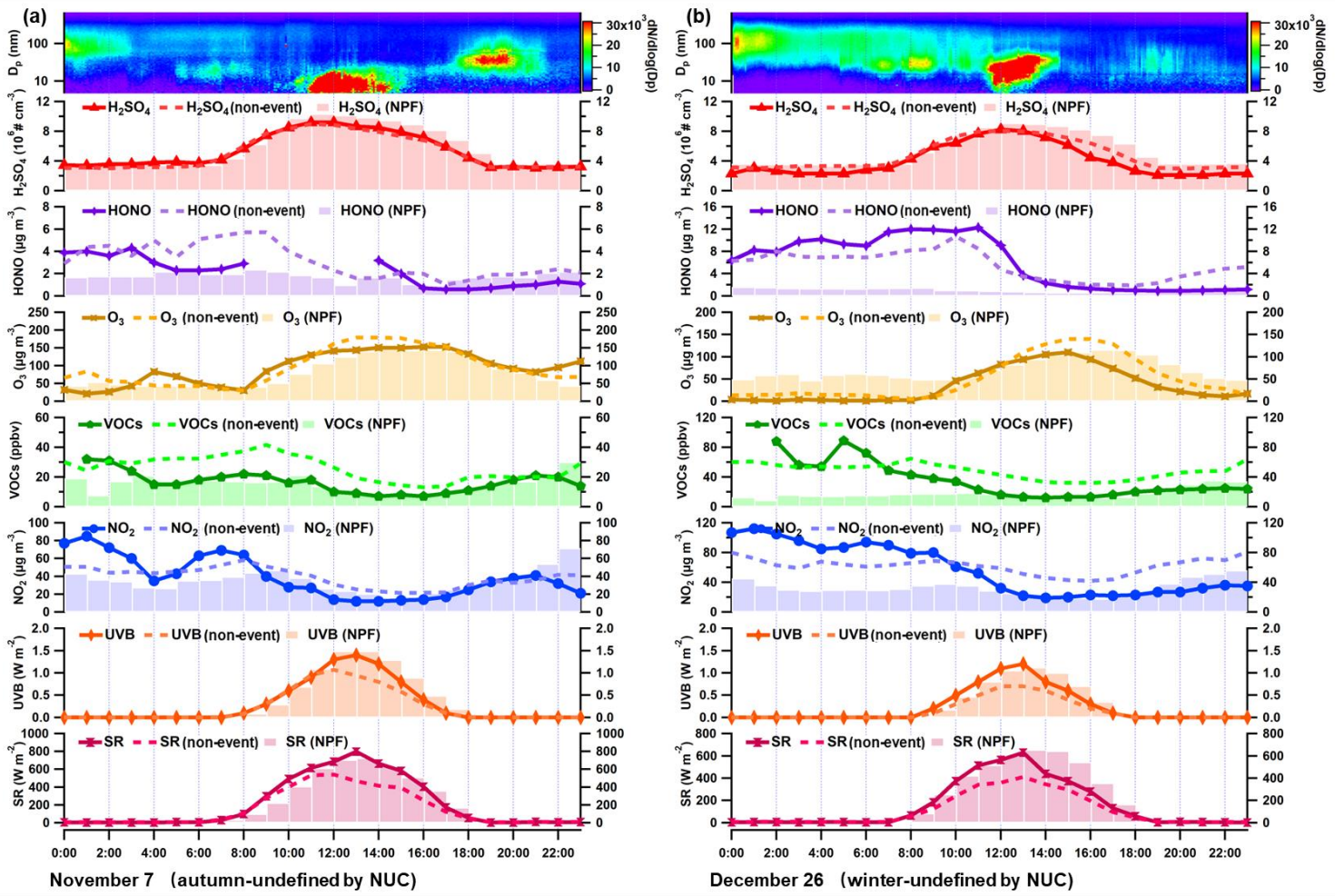
(a)
(b)
D_p (nm)
dN/dlog(D_p)
H_2SO_4
H_2SO_4 (non-event)
H_2SO_4 (NPF)
HONO
HONO (non-event)
HONO (NPF)
O_3
O_3 (non-event)
O_3 (NPF)
VOCs
VOCs (non-event)
VOCs (NPF)
NO_2
NO_2 (non-event)
NO_2 (NPF)
UVB
UVB (non-event)
UVB (NPF)
SR
SR (non-event)
SR (NPF)
November 7 (autumn-undefined by NUC)
December 26 (winter-undefined by NUC)

Fig.5

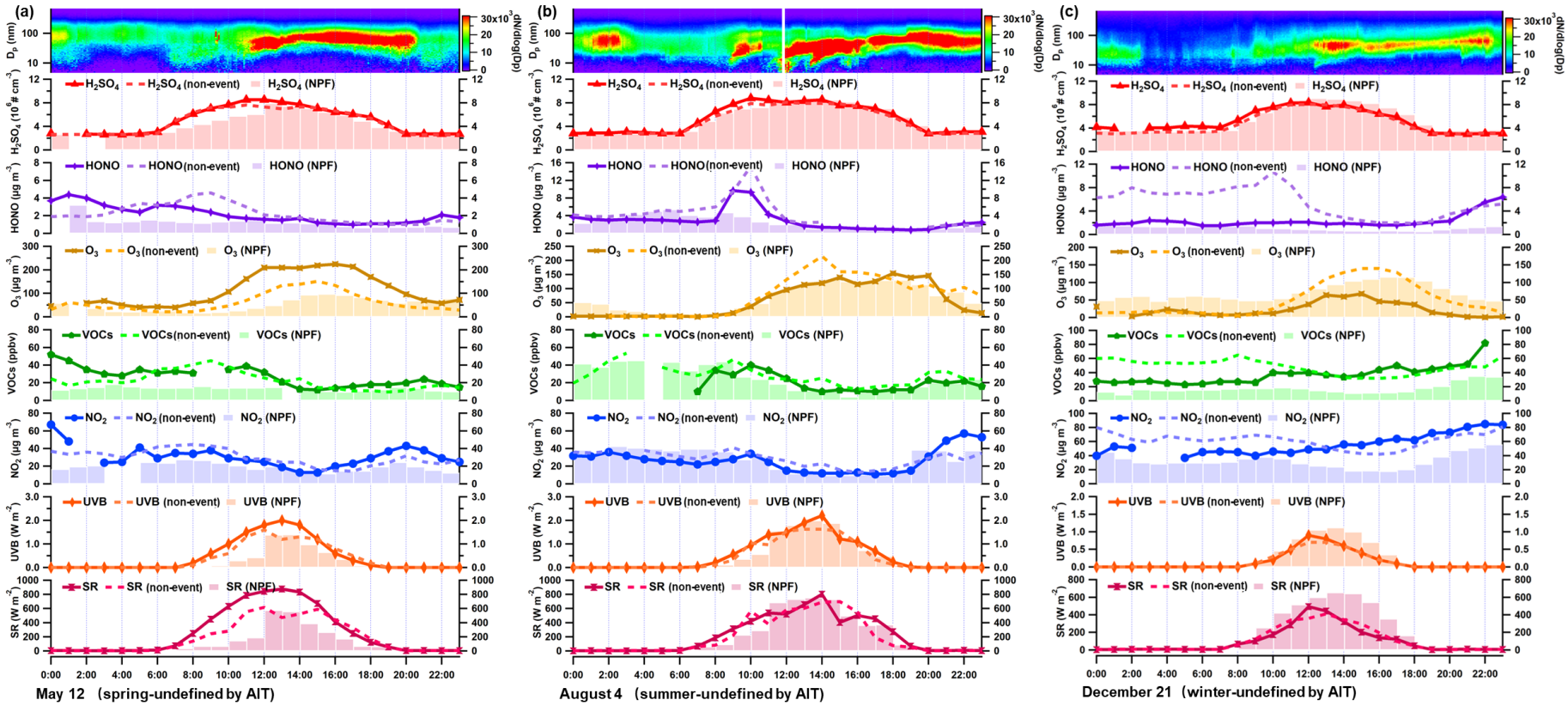
(a)
(b)
(c)
D_p (nm)
dN/dlog(Dp)
H_2SO_4 (10^6 # cm^{-3})
HONO (μg m^{-3})
O_3 (μg m^{-3})
VOCs (ppbv)
NO_2 (μg m^{-3})
UVB (W m^{-2})
SR (W m^{-2})
H_2SO_4
H_2SO_4 (non-event)
H_2SO_4 (NPF)
HONO
HONO (non-event)
HONO (NPF)
O_3
O_3 (non-event)
O_3 (NPF)
VOCs
VOCs (non-event)
VOCs (NPF)
NO_2
NO_2 (non-event)
NO_2 (NPF)
UVB
UVB (non-event)
UVB (NPF)
SR
SR (non-event)
SR (NPF)
May 12 (spring-undefined by AIT)
August 4 (summer-undefined by AIT)
December 21 (winter-undefined by AIT)

Fig.6

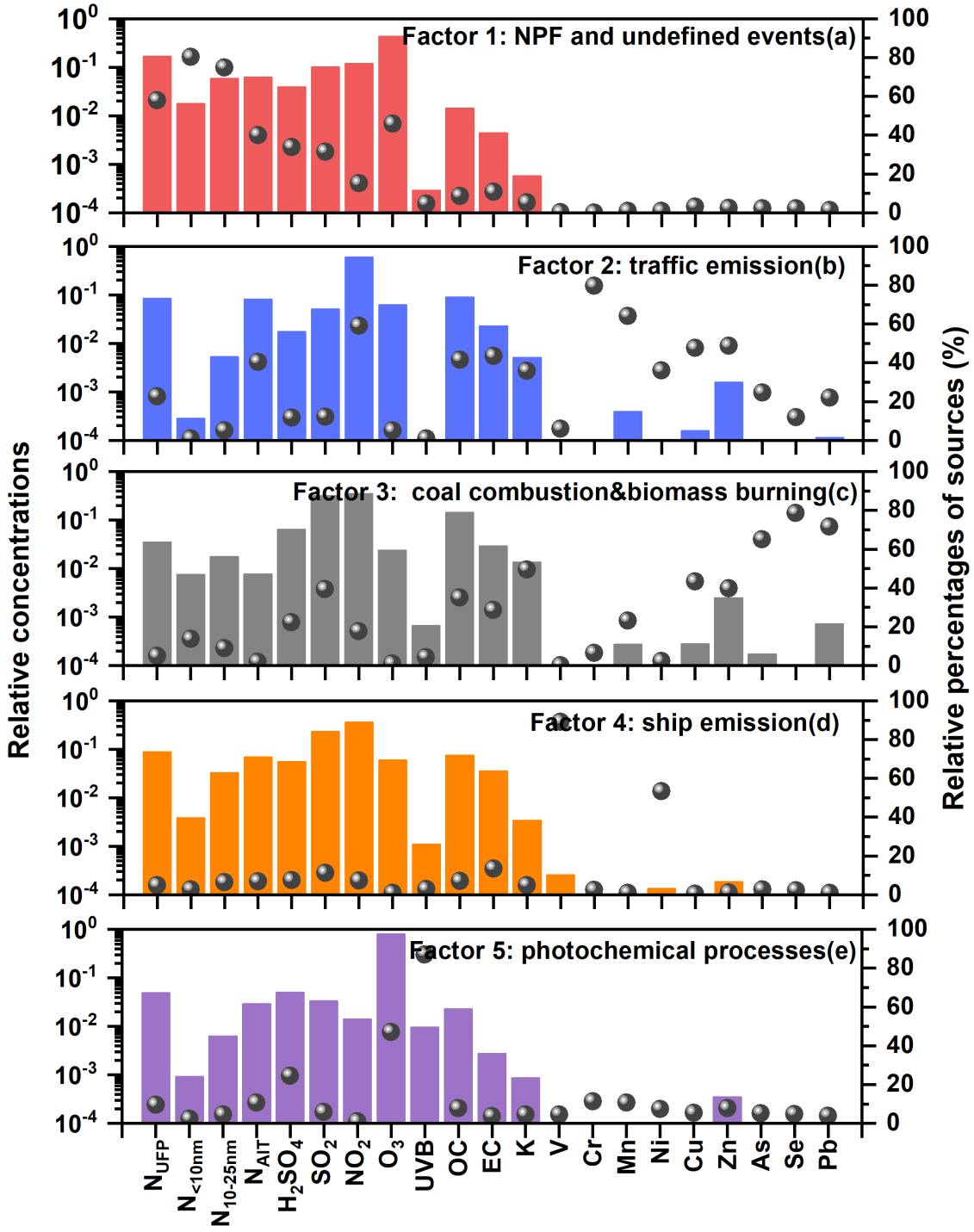
Factor 1: NPF and undefined events(a)
Factor 2: traffic emission(b)
Factor 3: coal combustion&biomass burning(c)
Factor 4: ship emission(d)
Factor 5: photochemical processes(e)
Relative concentrations
Relative percentages of sources (%)
N_UFP
N_<10nm
N_10-25nm
N_AIT
H2SO4
SO2
NO2
O3
UVB
OC
EC
K
V
Cr
Mn
Ni
Cu
Zn
As
Se
Pb

Fig.7

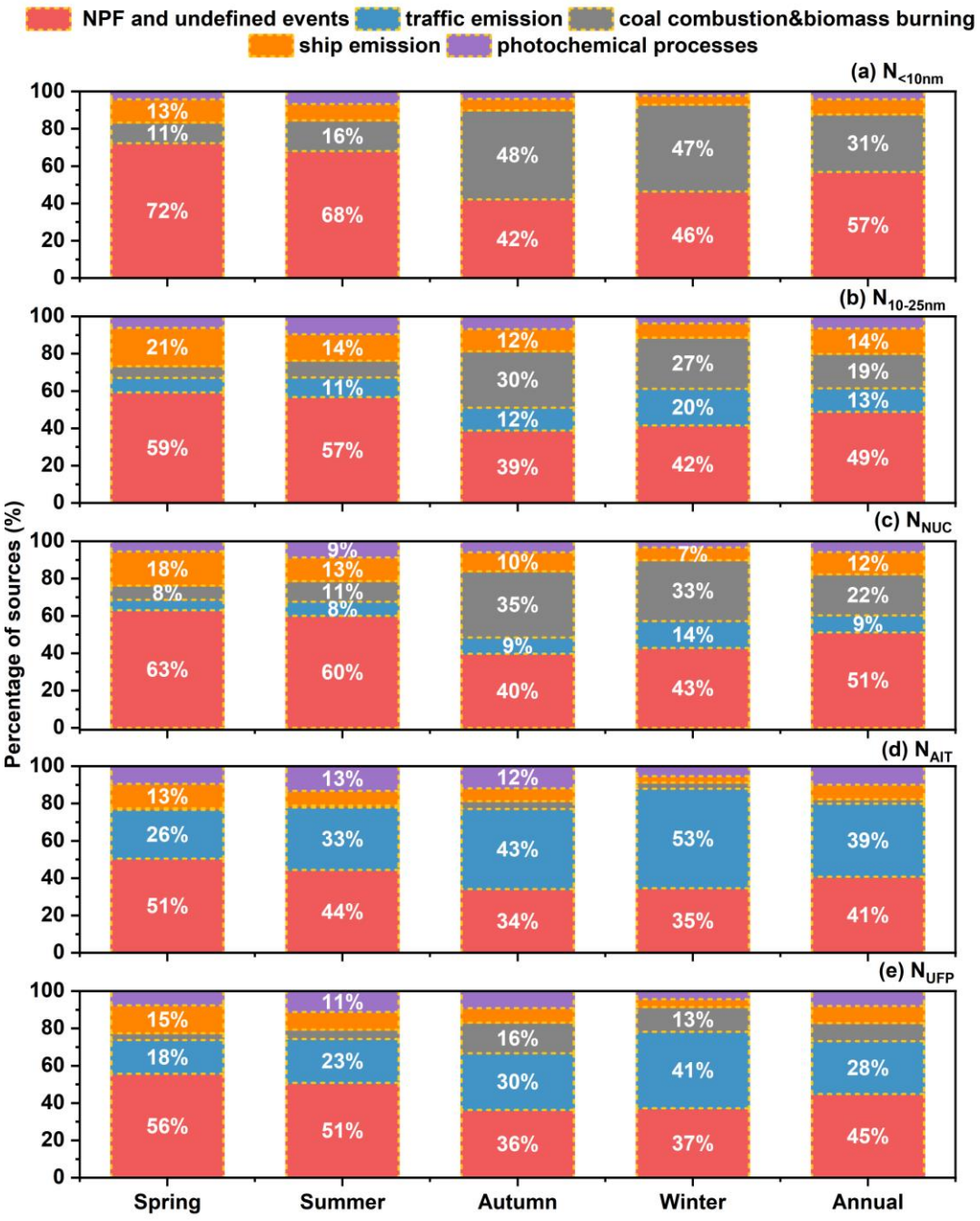
NPF and undefined events
traffic emission
coal combustion&biomass burning
ship emission
photochemical processes
(a) N<10nm
(b) N10-25nm
(c) NNUC
(d) NAIT
(e) NUFP
Percentage of sources (%)
Spring
Summer
Autumn
Winter
Annual

Fig.8


NPF and undefined events
traffic emission
coal combustion&biomass burning
ship emission
photochemical processes
(a) N<10nm
(b) N10-25nm
(c) NNUC
(d) NAIT
(e) NUFP
Percentage of sources (%)
0:00-2:00
3:00-5:00
6:00-8:00
9:00-11:00
12:00-14:00
15:00-17:00
18:00-20:00
21:00-23:00

Fig.9

Li Tao: Original draft preparation, Data curation; Zhen Zhou and Cheng Wu: Data curation and auxiliary data of pollutants processing; Jun Tao: Original draft preparation and Supervision; Leiming Zhang: Reviewing and Editing; Jiawei Li: WRF simulation; Dingli Yue, Zhijun Wu, Zhisheng Zhang and Boguang Wang: Reviewing; Ziyang Yuan and Junjun Huang: Data processing and Reviewing.

Conflict of interest statement

Dear Editor,

We declare that we have no financial and personal relationships with other people or organizations that can inappropriately influence our work, there is no professional or other personal interest of any nature or kind in any product, service and/or company that could be construed as influencing the position presented in, or the review of, the manuscript titled “High contribution of new particle formation to ultrafine particles in four seasons in an urban atmosphere in south China”.

Sincerely Yours,

Jun Tao and coauthors
Institute for Environmental and Climate Research, Jinan University, Guangzhou, China
Email: taojun@jnu.edu.cn